

1 Direct monitoring is revealing how submarine turbidity currents work

2
3 Talling P.J.¹, Cartigny, M.J.B.¹, Pope, E.¹, Baker, M.¹, Clare, M.A.², Heijnen³, M., Hage, S.
4 ⁴, Parsons, D.P.⁵, Simmons, S.M.⁵, Paull, C.K.⁶, Gwiazda, R.⁶, Lintern, G.⁷, Hughes Clarke,
5 J.E.⁸, Xu, J.⁹, Silva Jacinto, R.⁴, and Maier, K.L.¹⁰.

6
7 1. University of Durham, Durham, U.K.

8 2. National Oceanography Centre, Southampton, U.K.

9 3. University of Southampton, Southampton, U.K.

10 4. Geo-Ocean, University of Brest, CNRS, IFREMER, 29280 Plouzané, France.

11 5. University of Hull, Hull, U.K.

12 6. Monterey Bay Aquarium Research Institute, Moss Landing, California, U.S.A.

13 7. Geological Survey of Canada, Natural Resources Canada, Sidney, British Columbia V8L4B2, Canada.

14 8. University of New Hampshire, New Hampshire, U.S.A.

15 9. Southern University of Science and Technology, Guangdong, China.

16 10. National Institute of Water and Atmospheric Research, Te Whanganui-a-Tara Wellington, Aotearoa New
17 Zealand.

18 Corresponding author is Peter J. Talling Email: Peter.J.Talling@durham.ac.uk

19 20 **Abstract**

21 Seafloor sediment flows called turbidity currents form the largest sediment accumulations,
22 deepest canyons, and longest channels on Earth. It was once thought that turbidity currents
23 were impractical to measure in action, especially due to their ability to damage sensors in
24 their path. However, recent studies successfully monitored turbidity currents in detail, and
25 this review summarises resulting major advances in knowledge. Monitoring identifies new
26 triggering mechanisms from dilute river-plumes, and shows how rapid sediment
27 accumulation may precondition slope failure, but that the final triggers may be delayed and
28 subtle. Turbidity currents are consistently more frequent than predicted by past models,
29 including at sites located >300 km from any coast. Faster (> ~1.5 m/s) flows are driven by a
30 dense near-bed layer at their front, whilst slower flows are entirely dilute. This frontal layer
31 sometimes erodes very large volumes of sediment, yet maintains a near-uniform speed,
32 leading to a new model of behaviour. Monitoring shows how flows sculpt canyons and
33 channels via extremely fast-moving knickpoints, and how deposits originate. Emerging
34 technologies can now underpin widespread monitoring of turbidity currents, with lower costs

35 and risks, so that sediment and carbon fluxes due to turbidity currents can compare to other
36 major global transport processes.

38 **Introduction**

39
40 Turbidity currents are mixtures of sediment and water that travel downslope because they are
41 denser than the surrounding water [1]. They are fascinating due to their prodigious scale and
42 power (Fig. 1; Supplementary Table 1). For example, a turbidity current that broke all
43 telecommunication cables across the NW Atlantic in 1929 had a sediment volume of about
44 200 km^3 [2,3], which is ~ 30 times the global annual sediment flux from all rivers, and bigger
45 than the largest subaerial landslide in the last 350,000 years (Fig 1b; Supplementary Table 1).
46 These cable breaks showed the 1929 flow travelled at speeds of up to 19 m/s and ran out for
47 over 800 km (Fig. 1a) [2,3]. In 2020, turbidity currents initiated at the mouth of the Congo
48 River travelled for $> 1,100$ km through the Congo Submarine Canyon offshore West Africa
49 [4] (Fig. 1a). These flows accelerated from 5 to 8 m/s and eroded $\sim 2.65 \text{ km}^3$ of sediment (Fig.
50 1b). They broke both seabed telecommunication cables to West Africa, causing the internet to
51 slow from Nigeria to South Africa, just when capacity was most needed during Covid-19
52 related lockdowns [4,5].

53
54 Turbidity currents have wider importance for many reasons. As shown by the 1929 NW
55 Atlantic and 2020 Congo Canyon flows, turbidity currents commonly break networks of
56 seabed telecommunication cables [2-7] that now carry over 99% of global intercontinental
57 data traffic, as they have much greater bandwidth than satellites [7]. These cables form the
58 backbone of the internet, and they are critical for many aspects of our daily lives, from
59 intercontinental phone traffic to financial markets and cloud data storage [7]. Turbidity
60 currents also play an important role in transfer and burial of fresh organic carbon in marine
61 sediments, which remove CO_2 from the atmosphere, regulating climate over geologic time
62 scales [8-10] (Fig. 2b,c). It was once thought that terrestrial organic carbon supplied to the
63 oceans was mainly oxidized on continental shelves [11-13], and turbidity currents were
64 omitted from analyses of global carbon cycles [11-13]. However, recent work suggests burial
65 of terrestrial organic via turbidity currents can be highly efficient [8,9], and global estimates
66 of organic carbon burial in marine sediments may thus need to be revisited (Fig. 2b) [14].

68 Organic carbon is also the basis for all non-chemosynthetic marine food webs, and turbidity
69 currents may thus play a key role in functioning of seabed ecosystems [15,16]. Rapid and
70 sustained deposition of organic-carbon-rich sediment by turbidity currents can also favour
71 chemosynthetic communities [16], whilst sometimes extremely powerful flows may scour
72 life from the seafloor [5,17]. Turbidity currents and their carbon transport are linked to
73 human activities, as they can be generated by seabed trawling [18], or transfer microplastics
74 and other pollutants into the deep-sea [19]. Turbidity current deposits (called turbidites) also
75 provide a record of Earth history. This potentially includes long-term and therefore valuable
76 records of other important geohazards such as major earthquakes [20-22], or river-floods [4];
77 although it can be very challenging to infer the triggering mechanism for an ancient turbidite
78 with confidence. Thick and extensive turbidite deposits in the rock record also host major oil
79 and gas reserves in many locations worldwide [23].

80

81 Major advances in understanding have previously been made using analyses of rock outcrops,
82 seabed cores, and turbidity currents within laboratory experiments or numerical models [e.g.
83 1,24-26]. But the most remarkable aspect of submarine turbidity currents is how few direct
84 measurements we previously had from these flows [27-31], ensuring that they were poorly
85 understood [32]. Indeed, it was once thought to be impractical [33] to measure turbidity
86 currents directly in the oceans, due to their location, infrequent occurrence, and ability to
87 badly damage (or entirely remove) sensors left in their path.

88

89 However, over the last decade or so, a series of ambitious projects have used new sensors and
90 methods to provide the first detailed measurements within submarine turbidity currents (Fig.
91 4). They have consistently used acoustic Doppler current profilers (ADCPs) mounted on
92 moorings (Fig. 4e) to measure flow velocity profiles at frequencies of seconds to minutes,
93 including at multiple places along the flow pathway [34-53]. Projects were initially
94 conducted in shallow (< 500m) water [38,39], where logistics are easier and costs lower,
95 before moving into deeper (up to 2 km) water [35-37], and then finally capturing extremely
96 large events that reach water depths of 4-5 km [4] (Fig. 4b-d). Direct flow monitoring has
97 been combined with detailed time-lapse mapping of the seabed [35,38,39,54], tracking of
98 heavy objects (Fig. 4f) [35,52], sediment traps inside the flow [41-42,51], and coring of
99 seabed deposits [50,51] to make significant advances in our understanding of how turbidity
100 currents work. These projects have not been without challenges and risks, such as needing to
101 recover broken moorings drifting across the ocean surface near the Congo Canyon before

102 their locator beacons stopped transmitting, all during a Covid-19 related lockdown [4,5],
103 finding and recovering severed and buried cabled infrastructure [48], or when turbidity
104 currents occurred only on the last days of field campaigns [50].

106 This paper is the story of what recent direct monitoring studies can tell us about these
107 fascinating flows. It addresses some of the most fundamental questions about turbidity
108 currents, which include: (1) How are turbidity currents caused, and how reliably do they
109 record other major geohazards (e.g. earthquakes or floods)? (2) How frequent are turbidity
110 currents, and what are the wider implications for organic carbon cycles (Fig. 2)? (3) What are
111 turbidity currents: entirely dilute suspensions or driven by dense near-bed layers? (4) How do
112 flows evolve and behave? (5) How do flows sculpt the seafloor, and (6) how are turbidity
113 currents recorded by their deposits? It finishes with brief suggestions for key future work.

115 **Causes of turbidity currents**

117 Turbidity currents are caused by four general types of processes [55,56] (Fig. 5a). First,
118 turbidity currents can form from disintegration of underwater landslides [3,55,56] that may
119 have a variety of preconditioning factors (e.g. rapid sediment accumulation) and final triggers
120 (e.g. earthquakes or repeated wave loading). Second, turbidity currents may originate via
121 sediment-laden river discharge that is denser than seawater, and thus plunges to move along
122 the seabed as a 'hyperpycnal flow' [58] (Fig. 5a), although such conditions are rare. Third,
123 sediment settling from surface river plumes with much lower sediment concentrations than
124 hyperpycnal flows may generate turbidity currents [39,58] (Fig. 5a). Fourth, turbidity
125 currents can be initiated by oceanographic processes that transfer sediment to canyon heads,
126 which may be located far from river mouths [27,55,56]. Oceanographic processes include
127 storm waves and tides, or internal waves that move along density interfaces within the ocean
128 (Fig. 5a) [27,55,56].

130 Recent direct monitoring shows that generation of turbidity currents by surface river plumes
131 can occur at a far wider range of river mouths than once thought. It was previously believed
132 that it only occurred when sediment concentrations in rivers exceeded 1 kg/m^3 . However,
133 monitoring at Squamish Delta (Canada) showed that surface river plumes with sediment
134 concentrations as low as 0.07 kg/m^3 can generate frequent turbidity currents [39], sometimes
135 even more frequently than landslide-triggered turbidity currents [59]. This means that a much

136 larger fraction of river mouths globally have the potential to cause turbidity currents [39].
137 The exact mechanism by which turbidity currents originate below such dilute surface plumes
138 is still uncertain, but it may be linked to generation of mobile fluid-mud-like layers on the
139 seabed [39,47,48], or sediment trapping via estuarine circulation, or both [39].

140
141 Direct monitoring also shows that turbidity currents are caused in many locations by a
142 combination of river floods and tidal cycles (Fig. 5b-d), representing both riverine and
143 oceanographic processes. At both Squamish Delta and nearby Fraser Delta in British
144 Columbia, Canada, turbidity current activity switches on above a threshold river discharge,
145 and turbidity currents tend to occur at spring low-tides that produce stronger offshore directed
146 river plumes, in combination with easily remobilised seafloor mud layers [38,39,47,48].
147 Timing of exceptionally large turbidity currents in Congo Canyon offshore West Africa
148 show they are associated with major (1-in-50-year) river floods (Fig. 5c). However, these
149 turbidity currents finally occurred several weeks to months after the Congo River's flood
150 peak (Fig. 5c), typically at spring tides [4] (Fig. 5d).

151
152 Thus, there may be significant time delays after river floods before the turbidity currents are
153 eventually triggered (Fig. 5b). Submarine canyon heads can act as sediment 'capacitors',
154 which are later discharged, often due to a rather minor external perturbation such as spring
155 tides (fig. 5d) [4,60]. For example, multiple huge canyon-flushing flows in Congo Canyon
156 occurred several weeks or months after a river flood peak (Fig. 5c) [4], and a similar pattern
157 is seen elsewhere, albeit with shorter delays. For example, a turbidity current occurred 2-3
158 days after a huge flood along the Gaoping River in Taiwan [6], whilst landslide-triggered
159 turbidity currents occurred hours after the flood peak at the Squamish Delta [61]. It appears
160 that sediment builds up and stays on the seabed, before a final, often subtle trigger [4,60,61]
161 (Fig. 5b). Such delays therefore complicate the relationship between the timing of major
162 external events (e.g. floods and earthquakes) and turbidity currents. Indeed, in a few cases,
163 direct measurements shows that turbidity currents may be triggered without any obvious
164 synchronous external trigger. A turbidity current that moved at 4-7 m/s and ran out for 50 km
165 in Monterey Canyon occurred on a day without a storm, river flood or earthquake [60].

166
167 Triggers of 'canyon-flushing' events are especially important because it has been proposed
168 that deep-sea turbidites can record major earthquakes in some settings. If reliable, turbidite
169 paleo-seismology would be valuable, as these marine records can go back further in time than

170 almost all records on land [20-22]. However, care is needed as there are potential pitfalls.
171 Earthquake triggered turbidites need to be distinguished reliably from turbidites triggered in
172 many other ways, and we need to test whether all or only some major earthquakes trigger
173 distinctive turbidity currents [21,22]. It has been proposed that only earthquakes produce
174 synchronous turbidites over very extensive (>100 km) areas [20]. However, correlating
175 individual turbidite layers over such distances is challenging, especially for ancient layers if
176 uncertainties in radiocarbon dates are similar to earthquake recurrence intervals [20,22], and
177 tropical cyclones also affect very large areas [22]. Turbidites with multiple fining-upward
178 pulses have been linked to peaks in ground motion during earthquakes [20], but turbidity
179 currents with multiple pulses can also be generated by river floods [36,37,46]. Repeated
180 earthquake shaking may also potentially cause sediment to consolidate and become stronger
181 in some locations [62]. However, significant advances have been made in ‘testing the tests’
182 for earthquake triggered turbidites, and understanding which sites are better suited for
183 turbidite paleoseismology. For example, Howarth et al. [21] showed there was a consistent
184 spatial relationship between earthquake ground motions during the 2016 Kaikōura earthquake
185 and coseismic turbidites. McHugh et al. [63] also showed how the M_w 9 Tohoku-Oki
186 earthquake offshore Japan in 2011 remobilised a layer of surface sediment that was just a few
187 centimeters thick. Exceptionally well-dated turbidites in varved lakes can be correlated with
188 confidence and provide compelling evidence for earthquake triggering [64].

189
190 Direct monitoring also tests how turbidity currents may record major river floods [46,58]. At
191 least offshore from the Congo River, a single river flood may produce a cluster of multiple
192 turbidity currents in following years [4] (Fig. 5c). Direct monitoring of the Var system in the
193 Mediterranean showed how (non-earthquake) landslides and floods may produce turbidity
194 currents with multiple pulses, such that multi-pulsed deposits are not a unique criterion for
195 identifying earthquake or flood triggering [46]. Finally, turbidites may provide important
196 insights into how volcanic islands collapse [65], and whether this occurs in one or multiple
197 stages, which is critically important for tsunami magnitude.

198 199 **Flow frequency and its wider implications**

200
201 Direct monitoring of turbidity currents has consistently found that turbidity currents are more
202 frequent than previously expected (Fig. 3e; Supplementary Fig. 1), such as by sequence
203 stratigraphic models [66] (Fig. 3c,d). These sequence stratigraphic models infer that most

204 modern turbidity current systems are inactive, and that activity is mainly restricted to periods
205 of falling or low global sea-level (Fig. 3c) [66]. This is because post-glacial sea-level rise has
206 flooded continental shelves, causing almost all submarine canyon-heads to become detached
207 from river mouths (Fig. 3d), so that only ~180 of ~9,500 submarine canyons currently extend
208 to within 6 km of shore [67,68].

209
210 However, direct monitoring now shows that modern-day turbidity current systems in a range
211 of settings can be highly active. For example, over 100 turbidity currents occurred on
212 Squamish Pro-delta in Canada in ~3 months [38,39,59,61], whilst turbidity currents in the
213 upper Congo Canyon lasted for over a week (Supplementary Fig. 1d) and are active ~30% of
214 the time [36,37]. Turbidity currents occurred even in canyons fed by rocky shorelines that
215 lack obvious sediment sources [43]. More powerful canyon-flushing turbidity currents may
216 also be more frequent than once thought, as they can be linked to river floods with recurrence
217 intervals of a few decades (Fig. 5c) [4], as well as major earthquakes with longer recurrence
218 intervals [17]. Frequent and powerful flows were also measured outside of submarine
219 canyons and channels. For example, dozens of flows occurred on the open-slope of the Fraser
220 Pro-delta, some with velocities of > 6 m/s [47,48]. Most surprisingly, it was found that 4-6
221 powerful (5-8 m/s) flows occurred in Whittard Canyon each year, despite this canyon being
222 >300 km from the nearest shoreline [69] (Supplementary Fig. 1a-c). Indeed, Whittard Canyon
223 in the N.E. Atlantic is as active as Monterey Canyon in California, whose head is located tens
224 of meters from the shoreline [15,35]. There are several thousand other 'shoreline-detached'
225 canyons similar to Whittard Canyon [67,68], and this raises the question of their flow activity
226 [69].

227
228 Direct monitoring is thus consistent with some previous studies that challenged prevailing
229 models of dormant turbidity current systems during sea-level [e.g. 70] (Fig. 3d). Other lines
230 of evidence than direct monitoring also suggest that turbidity currents may transfer sediment
231 efficiently to the deep-sea, even when submarine canyon heads are not located within a few
232 kilometers of river mouths (Fig. 3e). Prograding wedges of sediment (clinoforms) offshore
233 from major rivers can reach canyon heads (Fig. 3e). This is the case for the huge Ganges-
234 Brahmaputra River that alone supplies ~16% of all riverine sediment to the ocean [71] (Fig.
235 2d), with dated cores showing a submarine canyon-head some 130 km from the river mouth
236 is highly active [72]. Oceanographic processes likely play a key role in producing these
237 highly active turbidity current systems located far from river mouths. For example, waves

238 and tides may resuspend sediment and transport it efficiently across continental shelves to
239 submarine canyons [73], as documented by studies of the continental shelf offshore from the
240 Eel River that show 70-80% of sediment was lost over the shelf edge (Fig. 3e) [74].

241
242 Thus, the present-day turbidity current 'pump' may be much more active than once thought
243 (Figs. 2 & 3e). This may have significant wider implications for transfer and burial of organic
244 carbon in the deep-sea [8,14], which affects atmospheric CO₂ levels and thus climate over
245 long (> 1,000 year) time scales [8,10,13,14]. Previous analyses of global carbon burial in the
246 oceans neglected the role of turbidity currents, assuming that terrestrial organic carbon
247 supplied by rivers was buried almost exclusively within deltas or continental shelves [11,12].
248 Past studies also inferred most terrestrial organic carbon was remineralised on continental
249 shelves, as occurs offshore from the Amazon River [11,12, 75], such that the global burial
250 efficiency of terrestrial organic carbon in marine sediments was low (10-44%) [11-13].
251 However, recent work suggested terrestrial organic burial by turbidity currents can be highly
252 efficient (>60-100%) in a wide range of settings [8,14]. They include the exceptionally large
253 Bengal Fan (Fig. 2d) [8], as well as fjords [76] and systems fed by small mountainous rivers
254 in Oceania [9]. This recently led to revised global estimates for mass-flux (~62-90 Mt C/yr)
255 and efficiency (31-45%) of terrestrial OC burial in marine sediments [14]. Photosynthesis in
256 the surface ocean produces a far greater (50,000 MtC/yr) amount of organic carbon [77], but
257 only 90-130 MtC/yr of that marine carbon is buried at the seabed (Fig. 2b) [10-14,77]. Thus,
258 burial flux of terrestrial organic carbon from turbidity currents approaches that due to settling
259 from the surface ocean [14], although only marine carbon produced via photosynthesis in the
260 surface ocean will affect atmospheric pCO₂ and thus climate on shorter term (<100 yr) time
261 scales (Fig. 2c) [78].

262
263 Almost all rivers would connect directly to submarine canyons during glacial low-stands
264 [67,68], so that global burial flux of terrestrial organic carbon will likely increase to >60-80%
265 [14]. This raises the possibility that terrestrial organic carbon burial by turbidity currents
266 varies systematically and substantially through glacial-interglacial cycles [79]. It is often
267 inferred that changes in surface ocean productivity further reduced atmospheric pCO₂ levels
268 during glacial periods [e.g. 78]. But more efficient terrestrial organic carbon burial by
269 turbidity currents could also have acted as a positive feedback to reduce atmospheric pCO₂
270 levels during glacials, albeit over much longer (> 1,000 years) timescales [79]. Thus, the
271 magnitude of change in organic carbon burial flux via turbidity currents between glacial and

272 inter-glacial periods (~30-95 Mt/yr) can rival changes in global organic carbon burial
273 proposed to drive other longer-term climate fluctuations [14]. For example, Li et al. [80]
274 inferred comparable changes in global organic carbon burial flux (~90 Mt/yr) were an
275 important positive feedback for global warming during the Neogene.

276
277 A more active turbidity current carbon pump may also have significant implications for
278 seabed life, as organic carbon underpins most marine food webs [81]. Turbidity currents also
279 physically disturb ecosystems by scouring the seabed, sometimes to depths of tens of meters,
280 or by depositing thick sediment layers that smother ecosystems [17]. Rapid accumulation of
281 organic-rich sediment can also lead to chemotrophic ecosystems resembling those around
282 black smokers [82]. Thus, impacts of turbidity currents on marine life warrant further
283 analysis.

284
285 Monitoring projects are also showing how human activities may trigger turbidity currents,
286 and thus impact wide areas of the seafloor. For example, it has been shown how bottom
287 trawling can both smooth (plough) the seabed, and initiate turbidity currents that travel down
288 canyons [18]. This canyon-monitoring work built upon previous remarkably determined
289 efforts to record how cold and dense water masses formed on continental shelves could
290 sometimes cascade down submarine canyons [83]. It took almost a decade of research cruises
291 to record these strong dense water cascades in action, but it showed how direct measurements
292 can lead to major advances [83]. More recently, it is being shown how turbidity currents may
293 disperse microplastic and other pollutants [19], or ventilate the deep ocean with warmer and
294 more oxygenated water [84].

295 296 **What turbidity currents comprise**

297
298 There has long been controversy over what turbidity currents comprise [1,26,86-86]. This
299 debate centres on whether they are entirely dilute and fully turbulent sediment suspensions, as
300 for most rivers, or driven by dense near-bed layers that resemble debris flows [86]. This
301 debate is not just in the detail; it is critical because the basic physics of dense or dilute
302 sediment flows are very different, and there is a need to know what type of flow to model in
303 the laboratory or numerically [86]. Geologists tried to answer this question by examining
304 turbidite deposits, but the answer is often ambiguous, especially when deposits comprise
305 massive or planar laminated sand (i.e. Bouma sequence divisions T_A and T_B) [86].

306

307 Detailed measurements from within turbidity currents thus play a key role in understanding
308 their internal nature (Fig. 6). They show the velocity structure of turbidity currents can differ
309 significantly from laboratory experiments, where a faster-moving body feeds a slower-
310 moving head (Fig. 6b) [33]. Measurements from the Congo Canyon show that turbidity
311 currents instead comprise a fast-moving frontal zone ('frontal cell') that outruns a much
312 slower-moving body, leading to flow stretching [36,37] (Fig. 6a,b). Such stretching might
313 explain the surprising week-long duration of Congo Canyon flows (Fig. 6a). Elsewhere, sand-
314 dominated turbidity currents also displayed a short-lived (< 30 min) frontal cell where
315 velocities are fastest (Fig. 6c), but these flows only lasted for minutes to hours (Fig. 6c;
316 Supplementary Fig. 1d) [34,35,41,45,46,50,53]. They lacked the sustained week-long body
317 seen in Congo Canyon flows (Fig. 5a), presumably because Congo Canyon flows contain
318 more mud that settles slowly [36,37].

319

320 There is also mounting evidence that faster (>1.5 m/s) turbidity currents contain denser near-
321 bed layers at their front, which drive the flow (Fig. 6) [35,38,40]. Multibeam echosounders
322 imaged denser near-bed layers at Squamish Delta (Canada) [38], but only in fast-moving
323 (>1.5 m/s) flows, although their exact sediment concentration is unknown. Transit (flow
324 front) velocities in Monterey Canyon were quicker than maximum velocities measured by
325 ADCPs (acoustic Doppler current profilers) inside the flow [35]. This was initially puzzling,
326 as the flow front must push through surrounding seawater that retards its progress. But
327 ADCPs typically do not measure within a few meters of the bed, and this suggest the
328 presence of a thin and fast layer near the bed [35]. Even more surprisingly, very heavy (up to
329 800 kg), dense (up to 6 g/cm³) and irregularly shaped objects (Fig. 4f) were carried for
330 several kilometres down Monterey Canyon at speeds of up to 4 m/s, comparable to maximum
331 flow speeds [35, 52]. These objects had different mass, densities and shapes, yet sometimes
332 moved together in lock step [35, 52]. Dense near-bed layers appear to have entombed and
333 rafted the heavy objects (Fig. 4f), and this is supported by a conductivity probe that dipped
334 close to the bed to record sediment volume concentrations of >11% [49]. Pope et al. [40] then
335 used an equation that predicts vertically-averaged sediment concentrations using
336 independently measured flow velocities and thicknesses, and a friction coefficient (Fig. 6c-e).
337 This Chezy-equation was applied to turbidity currents in Bute Inlet (Canada) to show that fast
338 (>1.5 m/s) flows were relatively dense (> ~10% and up to 38% sediment volume; Fig. 6c),
339 whilst slower moving flows were entirely dilute (Fig. 6e; [40]). The dense parts of flows

340 carry most of the sediment and drive the overall event [40], and they are likely characterised
341 by strongly damped turbulence and hindered settling, as well as grain-to-grain interactions.

342

343 Additional strong evidence shows that slower moving flows are entirely dilute (Fig. 6e). For
344 example, acoustic backscatter measurements from ADCPs can be used to derive sediment
345 concentrations, after making some assumptions about grain sizes [36, 37]. This method
346 concludes that the overlying sediment cloud and trailing body (Fig. 6a) typically has sediment
347 concentrations of just 0.1 to 0.001% by volume in the Congo Canyon [37].

348

349 Field evidence also supports a view that flows may evolve from having a dense near-bed
350 layer to become entirely dilute and fully turbulent as they decelerate [35,40]. For example,
351 dense near-bed layers were not observed by multibeam sonars in slower flows at Squamish
352 Delta [38], and objects were not carried for such long distances at more distal sites in
353 Monterey Canyon [35]. Pope et al. [40] used the Chezy-equation to show how flows evolved
354 from having a dense frontal layer to being entirely dilute as they decelerated (Fig. 6c-e).

355

356 **Behaviour of turbidity currents**

357

358 Submarine turbidity currents have been compared to terrestrial river systems, such as in the
359 way they produce meandering channels, but their behaviour differs in some fundamental
360 regards [24]. Unlike rivers, turbidity currents are driven by the weight of sediment they carry,
361 and density differences with surrounding seawater. Turbidity currents that erode the seabed
362 can therefore become denser and faster, causing even more erosion and acceleration,
363 producing a positive feedback termed ‘ignition’ (Fig. 7b) [25]. Alternatively, erosion and
364 deposition of sediment may be balanced, such that turbidity currents maintain a uniform
365 velocity and near equilibrium state (Fig. 7c) [4, 25]. Finally, deposition of sediment will
366 reduce flow densities and thus velocity, leading to further sediment settling, such that flows
367 dissipate (Fig. 7a).

368

369 Direct monitoring measurements can now test these basic hypotheses for how turbidity
370 currents behave. Detailed information on spatial changes in flow front speed is only available
371 from a handful of sites, but these datasets show a remarkably consistent pattern (Fig. 7d)
372 [4,40,87]. Flow behaviour tends to bifurcate, depending on initial velocities (Fig. 7d).

373 Initially faster-moving flows (>4-5 m/s) sustain near-uniform front velocities or gradually

374 accelerate, and thus runout much further [4,87]. Flows that initially travel at slower speeds
375 die out over much shorter distances (Fig. 7d) [4,87]. It is not yet clear why some flows (but
376 not others) reach these higher initial speeds, but it could result from initial remobilisation of
377 larger volumes of sediment, which then produces thicker and denser flows.

378

379 Three further key insights emerge from comparison of changes in flow speeds at different
380 sites (Fig. 7d). First, previous theory predicts sediment grain size and settling velocity should
381 have a strong impact on the threshold flow speed needed for either ignition or autosuspension
382 [25]. However, a similar threshold speed (4-5 m/s) occurs in sand-dominated (Monterey
383 Canyon) and mud-dominated (Congo Canyon) settings (Fig. 7d) [4,87]. The critical initial
384 speed needed for ignition or autosuspension therefore appears to be independent of the
385 settling velocity of individual grains, perhaps because faster flows have dense near-bed layers
386 where grains interact and do not settle individually. Second, although initial front speeds are a
387 good predictor of ignition-autosuspension, they are a poor predictor of runout distance, or
388 depth and volume of erosion. For example, flows with speeds of 5-8 m/s in Congo Canyon
389 ran out for > 1,100 km, and eroded a huge sediment volume, equivalent to 19-35% of the
390 annual flux from all rivers [4], whilst flows travelling initially at similar speeds in Monterey
391 Canyon ran out for >50 km, and caused little net erosion of the seabed (Fig. 7d) [35,52,87].
392 Third, although ignition may occur, it occurs gradually over long distances, and many flows
393 tend towards a near-uniform front speed (Fig. 7d). Indeed, flows in the Congo Canyon
394 combine elements of ignition (erosion of the seabed) and elements of autosuspension (near
395 uniform flow front speeds) [4].

396

397 This has led to a new 'travelling wave' model (Fig. 7e) for how turbidity currents evolve, in
398 which flows may be highly erosive (as for ignition) yet maintain near uniform speeds (as for
399 autosuspension) [4,87]. In this model, the event is driven by a dense, partially liquefied, near-
400 bed layer (travelling wave) at its front [4,87]. Erosion at the base of the dense layer, is
401 balanced by sediment deposition or transfer into a trailing dilute sediment cloud, leading to
402 near-uniform speeds (Fig. 7e). However, this model may not hold in unconfined settings,
403 such as basin plains, where very long (up to 2,000 km) runouts on low gradients (0.05°) can
404 occur without significant seabed erosion [86,88]. In such settings, slow settling cohesive mud
405 may provide the flow's main driving force. Indeed, mud may form vast fluid-mud layers that
406 only come to a halt and pond in bathymetric lows at the far end of deep-sea basins [86,89].

407

408 Observations in Monterey Canyon also point to the importance of seabed properties and
409 processes of sediment entrainment for turbidity current behaviour [87]. One of 16 flows
410 monitored in 2016-18 accelerated within the mid-canyon, and this was the only flow to occur
411 in summer months [87]. It seems most likely that this summer event either entrained a
412 seasonally developed weak mud-layer, or triggered local failure of the seabed, thereby
413 causing anomalous mid-canyon acceleration [87]. Time-lapse mapping of the Congo Canyon
414 also shows erosion of the seabed may be extremely patchy and localised on the canyon floor,
415 even where flows speeds remain relatively uniform [4,5]. Local areas of deep (20-30 m)
416 erosion are associated with waterfall-like features called knickpoints (Fig. 6). Indeed, cable
417 break observations worldwide show sequences of cables breaking and surviving, suggesting
418 uneven seabed erosion may be ubiquitous [4-6, 90]. It is not inevitable that a fast turbidity
419 current will break a cable. Cables that break may be located close to knickpoints, whereas
420 cables that survive are located away from knickpoints [4,5]. This could be tested by further
421 time-lapse mapping. Understanding and predicting rates of seabed erosion are a remaining
422 grand challenge, and it is critical for flow modelling, as patterns of erosion or deposition may
423 control flow behaviour [91].

424

425 **How turbidity currents sculpt the seabed**

426

427 Repeat (time lapse) mapping of the seabed is also providing major new insights into how
428 turbidity currents interact with the seabed [4, 17, 35, 38, 39, 43, 52, 57, 48, 54, 59, 92, 93]. It
429 is also showing how turbidity currents may differ in key regards from terrestrial rivers [25].
430 For example, flows exist in one of two basic states; supercritical flow is thinner and faster,
431 whilst subcritical flow is slower and thicker. A critical Froude number (Fr) separates
432 supercritical ($Fr > 1$) from subcritical ($Fr < 1$) flow, with this Froude number being
433 proportional to flow speed and inversely proportional to the density contrast between flow
434 and surrounding medium [94-97]. Subcritical flow occurs in most terrestrial rivers and
435 produces bedforms such as dunes and ripples that migrate down-slope. However, turbidity
436 currents are more prone to supercritical flow than rivers, due to their lower density contrast
437 with surrounding seawater, and often faster speeds [94-97]. There is indeed mounting
438 evidence that supercritical turbidity currents are widespread on the seafloor [98]. Spectacular
439 trains of up-slope migrating bedforms have been mapped on submarine canyon floors
440 worldwide [35,38,39], on open continental slopes [98], and flanks of volcanoes [99].
441 Combined flow monitoring and time-lapse seabed mapping has shown how these up-slope

442 migrating bedforms are linked to instabilities in supercritical flows [38,50], termed cyclic
443 steps, which lead to repeated alternations of supercritical and subcritical flow separated by
444 hydraulic jumps [94-97].

445
446 Time-lapse mapping is also showing how up-slope migrating knickpoints that are 10-30 m
447 high may dominate submarine channel-bend evolution (Supplementary Figure 2) [92].
448 Knickpoints can occur in river channels. However, their submarine cousins can be much
449 faster moving and migrate for hundreds of meters or more each year, driven by overpassing
450 turbidity currents [92, 93]. Knickpoints in rivers are caused by external processes such as
451 fault-uplift, sea-level variation and changes in bedrock, but this is not normally the case for
452 submarine knickpoints that are formed by internal processes such as cyclic steps or seabed
453 loading and failure [92]. These seabed knickpoints excavate submarine channels, whilst
454 depositing sediment in adjacent downstream areas (Supplementary Fig. 2) [92]. Knickpoints
455 also play a key role in how sediment, organic carbon and pollutants may be shuffled in
456 multiple stages to the deep-sea [100].

457
458 In meandering rivers, secondary (across-channel) flow at bends tends to sweep sediment
459 towards the inner-bank to form point bars [24]. However, vigorous debate has centred on
460 whether the secondary flow in turbidity currents occurs as in rivers, with near-bed flow
461 towards the inner-bank of a bend, or is reversed with near-bed flow towards the outer-bank
462 [24,101,102]. Flow monitoring at a bend in the Congo Canyon suggests that two secondary
463 flow cells occur, with near-bed flow sweeping sediment towards the outer bend [103]. But
464 knickpoint migration may be more important than secondary flow patterns for bend
465 evolution, at least in some settings (Supplementary Fig. 2) [92,100].

466
467 Turbidity currents were first proposed to explain the origin of huge underwater canyons that
468 were discovered in the 1800s on ocean and lake floors [1,104,105]. Available time-lapse
469 mapping currently only extends for a few decades at most [92,106], but it is starting to help
470 understand how these canyons form. For example, time-lapse mapping of the Kaikōura
471 Canyon offshore Aotearoa New Zealand, before and after a major (M_w 7.8) earthquake in
472 2016, shows how the earthquake caused widespread failure of the canyon-rim and other areas
473 [17]. This produced a turbidity current that caused gravel waves to move down-canyon and
474 eroded $> 1 \text{ km}^3$ of sediment, a volume that is 2-3 times the sediment entering the ocean
475 annually from Aotearoa rivers. This flow swept seabed life from a canyon that had one of the

476 highest benthic biomasses on Earth, and carried ~7 Mt of particulate organic carbon to the
477 deep-sea [17]. Time-lapse mapping of the Congo Canyon revealed that turbidity currents
478 eroded ~2.6 km³ of sediment in just one year, and flushed this sediment and associated
479 organic carbon into the deep-sea [4]. These repeat surveys show how fresh organic carbon
480 from river floods may be fast-tracked by turbidity currents, and explain how organic carbon
481 burial by turbidity currents may be highly efficient (Fig. 2b,d; Fig. 3) [8]. Time-lapse studies
482 have also showed how canyon-flank collapse may produce landslide-dams with implications
483 for sediment and organic carbon transfer. A ~0.09 km³ canyon-flank landslide dammed the
484 Congo Canyon, causing temporary storage of a further ~0.4 km³ of sediment with ~5 Mt of
485 (mainly terrestrial) organic carbon [106]. The trapped sediment was up to 150 m thick, and
486 extended >26 km up-canyon of the landslide-dam, and this dammed sediment is currently
487 being eroded and gradually released [106].

488

489 Meter-scale resolution seabed surveys are being collected using autonomous underwater
490 vehicles (AUVs) that fly at just a few tens of meters above the seabed, providing major new
491 insights into how submarine channel and fan systems operate [35, 43, 52, 107-110]. Previous
492 influential models of such systems assumed that channels bifurcated down-slope at their
493 termination, to form a distributary network, in the same way that many rivers bifurcate to
494 create deltas [111]. However, AUV mapping of submarine channel mouth terminations now
495 show that only a single main channel is active, although there may be fields of scours and
496 bedforms, as well as adjacent headless channels that fail to connect to the main channel
497 [109]. This channel mouth geomorphology is radically different to that seen in laboratory
498 experiments [112], and its significance for flow processes remains poorly understood.

499

500 **Understanding how deposits are formed**

501

502 Ancient turbidity current deposits (turbidites) form rock sequences in numerous locations
503 worldwide, which can be kilometers thick, and accumulate over thousands to millions of
504 years [111,113]. Geologists have proposed models for how flows and deposits are linked,
505 based on this rock record, but such models are difficult to test without observing the flow
506 itself [86]. Direct measurements from active flows are thus now being combined with
507 analysis of seabed cores to directly show how parent flows are recorded by their deposits.
508 These studies are producing major new insights, albeit only for processes operating over

509 rather short (days to a few years) time-scales, rather than longer term processes occurring
510 over thousands of years.

511

512 For example, seabed cores were combined with time-lapse mapping and direct flow
513 measurements to show how trains of cyclic step bedforms created by supercritical flows [38]
514 are recorded in deposits [50]. It showed how individual flow deposits comprising mainly
515 massive sand are linked to dense near-bed layers. Up-slope migration of single bedforms
516 initially produced backstepping stratal geometries, yet they were then eroded by migration of
517 subsequent bedforms with complex and offset crests to leave complex nested scours [50,114].
518

519 Time lapse mapping has also been used to understand completeness of turbidite deposits, and
520 how much of initially deposited sediment is finally preserved in the rock record. For example,
521 ~90 near-daily surveys spanning ~3 months [38] mapped patterns of erosion and deposition
522 offshore Squamish Delta [115]. They show that only 11% of sediment originally deposited
523 within channels was preserved, even on these very short (3 month) time scales [115]. Seabed
524 cores in Monterey Canyon were combined with direct flow measurements, as well as moored
525 traps that captured sediment from within the flow [51,81,98]. This work showed sand can be
526 restricted to a few meters above the canyon floor, and internal tides occurring between
527 turbidity currents stir up fine-mud, so that the fine-mud is poorly recorded in sand-dominated
528 canyon floor cores [51]. Organic carbon may also be kept in suspension, such that it is
529 underrepresented in seabed cores [81].

530

531 A puzzling feature of individual ancient turbidite beds is that they have a distinctly bimodal
532 distribution of thickness and internal deposit types [116]. Thicker (>40 cm) beds tend to
533 contain intervals of massive and planar laminated sand, whilst thin beds (<40 cm) tend to
534 comprise only ripple cross-laminated sand and overlying mud [116]. Long distance mapping
535 of individual turbidite deposits shows how flows may evolve from thick to thin beds, with a
536 relatively sharp termination of massive and planar-laminated intervals [86,117]. Direct
537 monitoring may now explain why turbidite deposits are bimodal [40]; faster flows contain a
538 dense near-bed layer that can deposit massive and planar-laminated sand, whilst slower flows
539 are entirely dilute and produce thinner turbidite deposits with cross-bedding (Fig. 6c,e) [40].

540

541 **Future directions**

542

543 There are now exciting opportunities to use direct monitoring data from turbidity currents to
544 test computational or analytical flow models, design more realistic laboratory flume
545 experiments, or understand deposits. Models and flume experiments need to simulate near-
546 bed layers with high (10-30%) sediment concentrations in faster ($> \sim 1.5$ m/s) flows. A key
547 challenge is to develop a robust theoretical framework for how such hyper-concentrated
548 layers behave, in which turbulence is damped strongly, grain settling is hindered, yet
549 deposition occurs incrementally rather than en-masse. This framework would be comparable
550 to that developed recently for even higher sediment concentration debris flows by Iverson
551 and others [119], where en-masse deposition occurs.

552

553 This review is also a rally call for widespread global monitoring of turbidity currents, over
554 longer timescales, and underpinned by a new generation of sensors that are deployed at
555 significantly lower cost and risk. The current situation is broadly comparable to trying to
556 understand how rivers work globally, using sporadic and incomplete monitoring from just
557 ~ 10 sites, mainly smaller streams. We need to study locations where occurrence of turbidity
558 currents would be more surprising, as shown by work in Whittard Canyon (Supplementary
559 Figure 1) [69], or other types of system such as those with hyperpycnal flows.

560

561 A key issue is that moored sensors tend to be broken by faster (> 5 m/s) turbidity currents [4,
562 118], such that other types of sensors are needed that can be placed outside the active flow,
563 and thus out of harm's way. Seismic signals (ground shaking) [120] or acoustic noise [121]
564 emitted by turbidity currents may underpin a new generation of sensors that remotely sense
565 turbidity currents from a safe distance. Indeed, an exciting development is that submarine
566 landslides may also be remotely sensed using seismic signals, at low cost, simultaneously
567 over large ocean basins. Fan et al. [122] use such signals to infer that 75 of the 85 landslides
568 that occurred in a 7-year period in the Gulf of Mexico were triggered by remote and
569 sometimes moderate earthquakes, which were hundreds or even thousands of kilometers
570 away [122]. Lower cost sensing systems are also needed that relay data back to base via
571 surface floats and satellites, rather than being retrieved by expensive vessels [118]. Without
572 these lower cost systems, we will only ever have funds to study just a few sites.

573

574 Currently, direct monitoring is good at measuring flow velocities (Fig. 6); yet the most
575 important parameter may be the flow's sediment concentration and density, as this is what
576 drives the flow [1], and determines sediment mass-flux. Future monitoring studies need to

577 focus on how to measure sediment concentration in turbidity currents, as well as how flows
578 erode the seabed, as mass-exchange with the bed often dominates overall flow behaviour
579 [91]. Methods to constrain mass fluxes, together with a more global monitoring network,
580 could then answer a remaining grand scientific challenge. This is to determine the global
581 sediment and organic carbon fluxes carried by turbidity currents, and their fundamental
582 controls, and therefore how these fluxes compare to other major global sediment and carbon
583 pumps on Earth (Fig. 2a-c).

584

585 **References**

- 586 [1] Kuenen, P.H. and Migliorini, C.I. Turbidity currents as a cause of graded bedding. *J.*
587 *Geol.* **58**, 91–127 (1950).
- 588 [2] Heezen B.C. & Ewing, M. Turbidity currents and submarine slumps, and the 1929 Grand
589 Banks earthquake. *Am. J. Science*, **250**, 849-873 (1952).
- 590 [3] Piper, D.J.W., Cochonat, P. & Morrison M.L. The sequence of events around the
591 epicenter of the 1929 Grand Banks earthquake: initiation of the debris flows and turbidity
592 current inferred from side scan sonar. *Sedimentology*, **46**, 79-97 (1999).
- 593 [4] Talling, P.J. et al.. Longest sediment flows yet measured show how major rivers connect
594 efficiently to deep-sea. *Nature Comms*, **13**, 4193 (2022).
- 595 [5] Talling, P.J. et al.. Flood and tides trigger longest measured sediment flow that accelerates
596 for thousand kilometers into deep-sea. A white paper on submarine cable geohazards
597 archived on Earthxiv. doi.org/10.31223/X5W328 (2022).
- 598 [6] Carter, L., Milliman, J., Talling, P.J., Gavey, R., & Wynn, R.B. Near-synchronous and
599 delayed initiation of long run-out submarine sediment flows from a record breaking river-
600 flood, offshore Taiwan. *Geophys. Res. Lett.* **39**, L12063 (2012).
- 601 [7] Carter, L., Gavey, R., Talling, P. & Liu, J. Insights into submarine geohazards from
602 breaks in Subsea Telecommunication Cables. *Oceanography* **27**, 58–67 (2014).
- 603 [8] Galy, V. et al. Efficient organic carbon burial in the Bengal fan sustained by the
604 Himalayan erosional system. *Nature* **450**, 407-410 (2007).
- 605 [9] Kao, S-J. et al. Preservation of terrestrial organic carbon in marine sediments offshore
606 Taiwan: mountain building and atmospheric carbon dioxide sequestration. *Earth Surf.*
607 *Dynam.* **2**, 127–139 (2014).
- 608 [10] Hilton, R.G. & West, A.J. Mountains, erosion and the carbon cycle. *Nature Reviews,*
609 *Earth & Environment* **1**, 284–299 (2020).

- 610 [11] Berner, R.A. 1989. Biogeochemical cycles of carbon and sulfur and their effect on
611 atmospheric oxygen over Phanerozoic time. *Palaeogeogr. Palaeoclimatol. Palaeoecol.* **73**,
612 97–122.
- 613 [12] Burdige, D.J. Burial of terrestrial organic matter in marine sediments: a reassessment.
614 *Glob. Biog. Cycles* **19**, GB4011 (2005).
- 615 [13] Blair, N.L. & Aller, R.C. 2012. The fate of terrestrial organic carbon in the marine
616 environment. *Annual Rev. Marine Sci.* **4**, 401–423.
- 617 [14] Talling, P.J., Hage, S., Baker, M.L., Bianchi, T.S., Hilton R.G., & Maier, K.L. The
618 global turbidity current pump and its implications for organic carbon cycling. *Ann. Revs.*
619 *Marine Sci.* in press (2023).
- 620 [15] Amaro, T. et al. The Whittard Canyon – A case study of submarine canyon processes.
621 *Progress in Oceanography* **146** (2016) 38–57.
- 622 [16] Rabouille, C., Baudin, F., Dennielou, B. & Olu, K. Organic carbon transfer and
623 ecosystem functioning in the terminal lobes of the Congo deep-sea fan: outcomes of the
624 Congolobe project. *Deep-sea Res. Part II* **142**, 1–6 (2017).
- 625 [17] Mountjoy, J.J. et al. Earthquakes drive large-scale submarine canyon development and
626 sediment supply to deep-ocean basins. *Sci. Adv.* **4**, eaar3748 (2018).
- 627 [18] Puig, P. et al. Ploughing the deep-sea floor. *Nature* **489**, 286–289 (2012).
- 628 [19] Kane, I.A. & Clare, M.A. Dispersion, accumulation, and the ultimate fate of
629 microplastics in deep-marine environments: a review and future directions. *Frontiers in Earth*
630 *Science* **7**, article 80 (2019).
- 631 [20] Goldfinger, C. Submarine paleoseismology based on turbidite records. *Annual Review of*
632 *Marine Science* **3**, 35–66 (2011).
- 633 [21] Howarth, J.D. et al. Calibrating the marine turbidite paleoseismometer using the 2016
634 Kaikōura earthquake. *Nature Geosci.* **14**, 161–167 (2021).
- 635 [22] Talling, P.J. Fidelity of turbidites as earthquake records. *Nature Geosci.* **14**, 113–116
636 (2021).
- 637 [23] Pettingill, H.S. & Weimer, P. Worldwide deepwater exploration and production: Past,
638 present, and future. *Leading Edge* **21**, 371 (2002).
- 639 [24] Peakall, J., & Sumner, E.J. Submarine channel flow processes and deposits: A process-
640 product perspective. *Geomorphology* **244**, 95–120 (2015).
- 641 [25] Parker, G., Fukushima, Y. & Pantin, H.M. Self-accelerating turbidity currents. *J. Fluid*
642 *Mech.*, **171**, 145–181 (1986).

- 643 [26] Lowe, D.R. Sediment gravity flows. 2. Depositional models with special reference to
644 high density turbidity currents. *J. Sedim. Petrol.*, **52**, 279-298 (1982).
- 645 [27] Inman, D.L., Nordstrom, C.E., & Reinhard, E.F. Currents in submarine canyons: an air-
646 sea-land interaction. *Ann. Rev. Fluid Mech* **8**, 275-310 (1976).
- 647 [28] Dill, R.F. Earthquake effects on fill of Scripps Submarine Canyon. *Geol. Soc. Am. Bull.*
648 **80**, 321-328 (1969).
- 649 [29] Hay, A.E., Burling, E.W., & Murray, J.W. Remote acoustic detection of a turbidity
650 current surge. *Science* **217**, 833-845 (1982).
- 651 [30] Bornhold, B.D., Ren, P., & Prior, D.B. High-frequency turbidity currents in British
652 Columbia fjords. *Geo-Mar. Letts* **14**, 238-243 (1994).
- 653 [31] Khripounoff, A. et al. Direct observation of intense turbidity current activity in the Zaire
654 submarine valley at 4000 m water depth. *Marine Geol.* **194**, 151-158 (2003).
- 655 [32] Talling, P.J. et al. Key future directions for research on turbidity currents and their
656 deposits. *J. Sedim. Res.* **85**, 153-169 (2015).
- 657 [33] Kneller, B., & Buckee, C. The structure and fluid mechanics of turbidity currents: a
658 review of some recent studies and their geological implications. *Sedimentology* **47**, 62-94
659 (2002).
- 660 [34] Xu, J. P., Noble, M. A., & Rosenfeld, L. K. In-situ measurements of velocity structure
661 within turbidity currents. *Geophys. Res. Lett.*, **31**, L09311 (2004).
- 662 [35] Paull, C.K. et al. Powerful turbidity currents driven by dense basal layers. *Nature*
663 *Communications* **9**, 4114 (2018).
- 664 [36] Azpiroz-Zabala, M. et al. Newly recognized turbidity current structure can explain
665 prolonged flushing of submarine canyons. *Sci. Advances* **3**, e1700200 (2017).
- 666 [37] Simmons, S.M. et al. Novel acoustic method provides first detailed measurements of
667 sediment concentration structure within submarine turbidity currents. *J. Geophy. Res.* **125**,
668 e2019JC015904.
- 669 [38] Hughes Clarke, J.E. First wide-angle view of channelized turbidity currents links
670 migrating cyclic steps to flow characteristics. *Nature Comms* **7**, 11896 (2016).
- 671 [39] Hage, S. et al. Direct monitoring reveals initiation of turbidity currents from extremely dilute
672 river plumes. *Geophy. Res. Letts* **46**, 11,310 - 11,320 (2019).
- 673 [40] Pope, E.L. et al. First source-to-sink monitoring shows dense head determines sediment
674 gravity flow runout. *Science Advances*, **8**, eabj3220 (2022).

- 675 [41] Liu, J.T., Kao, S.-J., Huh, C.-A., & Hung, C.-C. Gravity flows associated with flood
676 events and carbon burial: Taiwan as instructional source area. *Ann. Revs. Marine Science* **5**,
677 47–68 (2013).
- 678 [42] Liu, J.T. et al. Cyclone induced hyperpycnal turbidity currents in a submarine canyon. *J.*
679 *Geophys. Res.* **117**, C04033 (2012).
- 680 [43] Normandeau, A. et al. Storm-induced turbidity currents on a sediment-starved shelf:
681 Insight from direct monitoring and repeat seabed mapping of upslope migrating bedforms.
682 *Sedimentology* **67**, 1045–1068 (2020).
- 683 [44] Xu, J.P., Swarzenski, P.W., Noble, M., & Li, A.-C. Event-driven sediment flux in
684 Hueneme and Mugu submarine canyons, Southern California. *Marine Geology* **269**, 74–88
685 (2010).
- 686 [45] Khripounoff, A., Crassous, P., Lo Bue, N., Dennielou, B., & Silva Jacinto, R. Different
687 types of sediment gravity flows detected in the Var submarine canyon (northwestern
688 Mediterranean Sea): *Prog. Oceanography* **106**, 138–153 (2012).
- 689 [46] Heerema, K. et al. How distinctive are flood-triggered turbidity currents? *J. Sedim. Res.*
690 **92**, 1–11 (2022).
- 691 [47] Lintern, D.G., Hill, P.R. & Stacey, C. Powerful unconfined turbidity current captured by
692 cabled observatory on the Fraser River delta slope, British Columbia, Canada. *Sedimentology*
693 **63**, 1041–1064 (2016).
- 694 [48] Hill, P.R. & Lintern, D.G. Turbidity currents on the open slope of the Fraser Delta.
695 *Marine Geology* **445**, 106738 (2022).
- 696 [49] Wang, Z. et al. Direct evidence of a high-concentration basal layer in a submarine
697 turbidity current. *Deep-sea Res. Part I* **161**, 103300 (2020).
- 698 [50] Hage, S. et al. How to recognize crescentic bedforms formed by supercritical turbidity
699 currents in the rock record: insights from active submarine channels. *Geology* **6**, 563-566
700 (2018).
- 701 [51] Maier, K.L. et al. Linking direct measurements of turbidity currents to submarine
702 canyon-floor deposits. *Front. Earth Sci. (Sedimentology, Stratigraphy and Diagenesis)*. doi:
703 10.3389/feart.2019.00144 (2019).
- 704 [52] Meng, L., Wang, Z., & Xu, J. Two distinct types of turbidity currents observed in
705 the Manila Trench, South China Sea. *Commun Earth Environ* **4**, 108 (2023).
- 706 [53] Gwiazda, R. et al. Near-bed structure of sediment gravity flows measured by motion-
707 sensing 'boulder-like' Benthic Event Detectors (BEDs) in Monterey Canyon. *J. Geophys. Res.*
708 **127** (2022).

- 709 [54] Hill, P. Changes in submarine channel morphology and slope sedimentation patterns
710 from repeat multibeam surveys in the Fraser River delta, western Canada. *Int. Assoc.*
711 *Sedimentol. Spec. Pub.* **44**, 47–70 (2012).
- 712 [55] Talling, P.J., Paull, C.K. & Piper, D.J.W. How are subaqueous sediment density flows
713 triggered, what is their internal structure and how does it evolve? Direct observations from
714 monitoring of active flows. *Earth Sci. Revs* **125**, 244-287 (2014).
- 715 [56] Piper, D.J.W. & Normark, W.R. Processes that initiate turbidity currents and their
716 influence on turbidites: a marine geology perspective. *J. Sedim. Res.* **79**, 347–362 (2009).
- 717 [57] Clare, M.A. et al. Direct monitoring of active geohazards: emerging geophysical tools
718 for deep-water assessments. *Near Surf. Geophys* **15**, 427-444 (2017).
- 719 [58] Mulder, T., Syvitski, J.P.M., Mignone, S., Faugeres, J.C. & Savoye, B. Marine
720 hyperpycnal flows: initiation, behaviour, and related deposits. A review. *Mar. Petrol. Geol.*,
721 **20**, 861-882 (2003).
- 722 [59] Hizzett, J. L. et al. Which triggers produce the most erosive, frequent and longest runout
723 turbidity currents on deltas? *Geophys. Res. Letts* **45**, 855-863 (2017).
- 724 [60] Bailey, L.P. et al. Preconditioning by sediment accumulation can produce powerful
725 turbidity currents without major external triggers. *Earth & Planetary Sci. Letts* **562**,
726 art.116845 (2021).
- 727 [61] Clare, M.A., Hughes Clarke, J.E., Talling, P.J., Cartigny, M.J. & Pratomo, D.G.
728 Preconditioning and triggering of offshore slope failures and turbidity currents revealed by
729 most detailed monitoring yet at a fjord-head delta. *Earth & Planet. Sci. Letts* **450**, 208-220
730 (2016).
- 731 [62] Sawyer, D. & DeVore, J. Evidence for seismic strengthening from undrained shear
732 strength measurements. *Geophys. Res. Letts* **42**, 10,216-10,221(2016).
- 733 [63] McHugh, C.M. et al. Remobilization of surficial slope sediment triggered by the A.D.
734 2011 M_w9 Tohoku- Oki earthquake and tsunami along the Japan Trench. *Geology* **44**, 391–
735 394 (2016).
- 736 [64] Moernaut, J. et al. Lacustrine turbidites as a tool for quantitative earthquake
737 reconstruction: New evidence for a variable rupture mode in south central Chile. *J. Geophys.*
738 *Res.* **119**, 1607–1633 (2014).
- 739 [65] Hunt, J.E., Wynn, R.B., Masson, D.G., Talling, P.J., & Teagle, D.A. Sedimentological
740 and geochemical evidence for multistage failure of volcanic island landslides: a case study
741 from Icod landslide on north Tenerife, Canary Islands. *G-cubed*, GC003740 (2011).

- 742 [66] Posamentier, H.W., Erksine, R.D. & Mitchum, R.M., Jr. Submarine fan deposition
743 within a sequence stratigraphic framework, in Welmer, B., and Link, M.H., eds., Seismic
744 facies and sedimentary processes of submarine fans and turbidite systems: New York,
745 Springer Verlag, 127–136 (1991).
- 746 [67] Harris, P. T. & Whiteway, T. Global distribution of large submarine canyons:
747 Geomorphic differences between active and passive continental margins. *Mar. Geol.* **285**,
748 69–86 (2011).
- 749 [68] Bernhardt, A. & Schwanghart, W. Where and why do submarine canyons remain
750 connected to the shore during sea-level rise? Insights from global topographic analysis and
751 Bayesian regression. *Geophys. Res. Lett.* **48**, e2020GL092234 (2021).
- 752 [69] Heijnen, M.S. et al. Challenging the highstand-dormant paradigm for land-detached
753 submarine canyons. *Nature Comms* **13**, 3448 (2022).
- 754 [70] Covault, J. A. & Graham, S. A. Submarine fans at all sea-level stands: Tectono-
755 morphologic and climatic controls on terrigenous sediment delivery to the deep-
756 sea. *Geology* **38**, 939-942 (2010).
- 757 [71] Milliman, J. D. & Farnsworth, K. L. River discharge to the coastal ocean: a global
758 synthesis, Cambridge University Press (2011).
- 759 [72] Rogers, K.G., Goodbred Jr., S.L. & Khan, S.R. Shelf-to-canyon connections: Transport-
760 related morphology and mass balance at the shallow-headed, rapidly aggrading Swatch of No
761 Ground (Bay of Bengal). *Marine Geology* **369**, 288–299 (2015).
- 762 [73] Wright, L.D., Friedrichs, C.T., Kim, S.C., & Scully, M.E. Effects of ambient currents
763 and waves on gravity-driven sediment transport on continental shelves. *Marine Geol.* **175**,
764 25–45 (2001).
- 765 [74] Wheatcroft, R.A., & Sommerfield, C.K. River sediment flux and shelf sediment
766 accumulation rates on the Pacific Northwest margin. *Cont. Shelf Res.* **25**, 311–332 (2005).
- 767 [75] Aller, R.C. & Blair, N.E. Carbon remineralization in the Amazon–Guianas mobile
768 mudbelt: a sedimentary incinerator. *Cont. Shelf Res.* **26**, 2241–2259 (2006).
- 769 [76] Smith, R., Bianchi, T., Allison, M., Savage, C. High rates of organic carbon burial in
770 fjord sediments globally. *Nature Geosci.* **8**, 450–453 (2015).
- 771 [77] Dunne, J.P., Darmiento, J.L. & Gnanadesikan, A. Synthesis of global particle export
772 from the surface ocean and cycling through ocean interior and on the seafloor. *Glob. Biog.*
773 *Cycl.* **21**, GB4006 (2007).
- 774 [78] Sundquist, E.T. The global carbon-dioxide budget. *Science* **259**, 934-941.

- 775 [79] Cartapanis, O., Galbraith, E.D., Bianchi, D. & Jacard, S.L. Carbon burial in deep-sea
776 sediment and implications for oceanic inventories of carbon and alkalinity over the last
777 glacial cycle. *Clim. Past.* **14**, 1819–1850 (2018)
- 778 [80] Li, Z., Zhang, Y.G., Torres, M., Mills, B.J.W. Neogene burial of organic carbon in the
779 global ocean. *Nature* **613**, 90-95 (2023).
- 780 [81] Maier, K.L. et al. Sediment and organic carbon transport and deposition driven by
781 internal tides along Monterey Canyon, offshore California. *Deep-sea Res.* **153**, 103108
782 (2019).
- 783 [82] Karine, O., Decker, C., Pastor, L., Caprais, J-C., Khrpounoff, A., Morioneaux, M., Ain,
784 B., Menot, L., & Rabouille, C. Cold-seep-like macrofaunal communities in organic- and
785 sulfide-rich sediments of the Congo deep-sea fan. *Deep Sea Res.* **142**, 180-196 (2017)
- 786 [83] Canals, M. et al. Flushing submarine canyons. *Nature* **444**, 354–357 (2006).
- 787 [84] Kao, S.J. et al. 2010, Cyclone driven deep-sea injection of freshwater and heat by
788 hyperpycnal flow in the subtropics. *Geophys. Res. Letts* **37**, L21702.
- 789 [85] Shanmugam, G. and R.J. Muiola. Reinterpretation of depositional processes in a classic
790 flysch sequence (Pennsylvanian Jackfork Group), Ouachita Mountains, Arkansas and
791 Oklahoma. *AAPG Bulletin*, **79**, 672-695 (1995).
- 792 [86] Talling, P.J., Sumner, E.J., Masson, D.G. & Malgesini, G. Subaqueous sediment density
793 flows: depositional processes and deposit types. *Sedimentology* **59**, 1937-2003 (2012).
- 794 [87] Heerema, C.J. et al. What determines the downstream evolution of turbidity currents?
795 *Earth & Planetary Sci. Letts.* **532**, 116023 (2020).
- 796 [88] Talling P. J. et al. Onset of submarine debris flow deposition far from original giant
797 landslide. *Nature* **450**, 541-544 (2007).
- 798 [89] McCave, I.N. & Jones, K.P.N. Deposition of ungraded muds from high-density non-
799 turbulent turbidity currents. *Nature* **133**, 250-252 (1988).
- 800 [90] Gavey, R. et al. Frequent sediment density flows during 2006 to 2015 triggered by
801 competing seismic and weather cycles: observations from subsea cable breaks off southern
802 Taiwan. *Marine Geol.* **384**, 147-158 (2017).
- 803 [91] Traer, M.M., Hilley, G.E., Fildani, A. & McHargue, T. The sensitivity of turbidity
804 currents to mass and momentum exchanges between these underflows and their surroundings.
805 *J. Geophys. Res.* **117**, F01009 (2012).
- 806 [92] Heijnen et al. Rapidly-migrating and internally-generated knickpoints can control
807 submarine channel evolution. *Nature Comms.* **11**, 3129 (2020).

- 808 [93] Chen, Y. et al. Knickpoints and crescentic bedform interactions in submarine channels.
809 *Sedimentology* **69**, 1358-1377 (2021).
- 810 [94] Kostic, S. & Parker, G. The response of turbidity currents to a canyon-fan transition:
811 hydraulic jumps and depositional signatures. *J. Hydraul. Res.* **44**, 631–653 (2006).
- 812 [95] Covault, J.A., Kostic, S., Paull, C.K., Ryan, H.F. & Fildani, A. Submarine channel
813 initiation, filling and maintenance from sea-floor geomorphology and morphodynamic
814 modelling of cyclic steps. *Sedimentology* **61**, 1031–1054 (2014).
- 815 [96] Cartigny, M.J.B., Ventra, D., Postma, G. & Van den Berg, J.H. Morphodynamics and
816 sedimentary structures of bedforms under supercritical-flow conditions: new insights from
817 flume experiments. *Sedimentology* **61**, 712–748 (2014).
- 818 [97] Slooman, A. & Cartigny, M.J.B. Cyclic steps: Review and aggradation-based
819 classification. *Earth Science Revs.* **201**, 102949 (2020).
- 820 [98] Symons, W.O., Sumner, E.J., Talling, P.J., Cartigny, M.J.B., Clare, M.A. Large-scale
821 sediment waves and scours on the modern seafloor and their implications for the prevalence
822 of supercritical flows. *Marine Geology* **371**, 140-178 (2016).
- 823 [99] Pope, E.L. et al. Origin of spectacular fields of submarine sediment waves around
824 volcanic islands. *E.P.S.L.*, 493, 12-24 (2018).
- 825 [100] Heijnen, M.S. et al. Fill, flush or shuffle: How is sediment carried through submarine
826 channels to build lobes? *Earth & Planet. Sci. Letters* **584**, Art. 117481 (2022).
- 827 [101] Corney, R. K. T. et al. The orientation of helical flow in curved channels.
828 *Sedimentology* **53**, 249–257 (2006).
- 829 [102] Imran, J. et al. Helical flow couplets in submarine gravity under-flows. *Geology* **35**,
830 659–662 (2007).
- 831 [103] Azpiroz-Zabala, M. et al. A general model for the helical structure of geophysical flows
832 in channel bends. *Geophys. Res. Letts.* 56721 (2017).
- 833 [104] Daly, R. A. Origin of submarine “canyons”. *American J. Sci.* **31**, 401–420 (1936).
- 834 [105] Forel, F-A. Les ravins sous-lacustres des fleuves glaciaires. *Comptes rendus de*
835 *l’académie des sciences de Paris*: 1-3 (1885).
- 836 [106] Pope, E.L. et al. Landslide-dams affect sediment and carbon fluxes in deep-sea
837 submarine canyons. *Nature Geosci.* 15, 845–853 (2022).
- 838 [107] Maier K.L. et al. Submarine fan development revealed by integrated high-resolution
839 datasets from La Jolla Fan, offshore California. *J. Sedim. Res.* 90, 468–479 (2020).
- 840 [108] Paull, C.K. et al. Anatomy of the La Jolla submarine canyon system: offshore southern
841 California. *Marine Geology* **335**, 16-34 (2013).

- 842 [109] Hodgson, D.M., Peakall, J. & Maier, K.L. Submarine channel mouth settings:
843 processes, geomorphology, and deposits. *Front. Earth Sci.* 10:790320 (2022).
- 844 [110] Wolfson-Schwehr, M., Paull, C.K., Caress, D.W., Gwiazda, R., Nieminski, N.M.,
845 Talling, P.J., Carvajal, C., Simmons, S., Troni, G. Time-lapse seafloor surveys reveal how
846 turbidity currents and internal tides in Monterey Canyon interact with the seabed at
847 centimeter-scale. *J. Geophys. Res* **128**, e2022JF006705 (2023).
- 848 [111] Mutti, E., Bernoulli, D., Ricci-Lucchi, F., & Tinterri, R. Turbidites and turbidity
849 currents from alpine 'flysch' to the exploration of continental margins. *Sedimentology* **56**,
850 267-318 (2009).
- 851 [112] Baas, J.H., Van Kesteren, W., & Postma, G. Deposits of depletive high-density
852 turbidity currents: a flume analogue of bed geometry, structure and texture. *Sedimentology*
853 **51**, 1053-1088 (2004).
- 854 [113] Nielsen T., R.D. Shew, G.S. Steffens & J.R.J. Studlick. Atlas of Deepwater Outcrops,
855 A.A.P.G. Studies in Geology 56, Shell Exploration and Production and A.A.P.G., 504 p
856 (2007).
- 857 [114] Englert, R.G. et al. Quantifying the three-dimensional stratigraphic expression of cyclic
858 steps by integrating seafloor and deep-water outcrop observations. *Sedimentology* **68**, 1465–
859 1501 (2021).
- 860 [115] Vendettuoli, D. et al. Daily bathymetric surveys document how stratigraphy is built
861 and its extreme incompleteness: One summer offshore Squamish Delta, British Columbia.
862 *Earth & Planet. Sci. Letts* **515**, 231-247 (2019).
- 863 [116] Talling, P.J. On the frequency distribution of turbidite thickness: *Sedimentology* 48,
864 1297-1329 (2001).
- 865 [117] Malgesini, G. et al. Quantitative analysis of submarine-flow deposit shape in the
866 Marnoso-Arenacea Formation: what is the signature of hindered settling from dense near-bed
867 layers? *J. Sedim. Res.* **85**, 170-191 (2015).
- 868 [118] Clare, M. et al. Lessons learned from monitoring of turbidity currents and guidance for
869 future platform designs. *Geol. Soc. Lond., Spec. Pub.* 500, [https://doi.org/10.1144/SP500-](https://doi.org/10.1144/SP500-2019-173)
870 2019-173 (2020).
- 871 [119] Iverson, R.M., Logan, M., LaHusen, R.G., & Berti, M. The perfect debris flow?
872 Aggregated results from 28 large-scale experiments. *J. Geophys. Res.* **115**, F03005 (2010).
- 873 [120] Baker, M., Virtual Bouma Conference abstract (2022).
- 874 [121] Hay, A.E., Hatcher M. G., & Hughes Clarke, J.E. Underwater noise from submarine
875 turbidity currents. *JASA Express Lett.* 1, 070801 (2021).

- 876 [122] Fan, W., McGuire J.J., & Shearer, P.M. Abundant spontaneous and dynamically
877 triggered submarine landslides in the Gulf of Mexico. *Geophys. Res. Letts.* **47**,
878 e2020GL087213 (2020).
- 879 [123] Covault, J. A. Submarine fans and canyon-channel systems: A review of processes,
880 products, and models. *Nature Education Knowledge* **3**(10), 4 (2011).
- 881 [124] Baudin, F., Rabouille, C., & Dennielou, B. Routing of terrestrial organic matter from
882 the Congo River to the ultimate sink in the abyss: a mass balance approach. *Geologica*
883 *Belgica* **23/1-2**, 41-52 (2020).
- 884 [125] Martin, J., Palanques, A., Vitorino, J., Oliveira, A., & de Stigter, H.C. Near-bottom
885 particulate matter dynamics in the Nazaré submarine canyon under calm and stormy
886 conditions. *Deep-Sea Res. II* **58**, 2388-2400 (2011).
- 887 [126] Lambert, A. & Giovanoli, F. Records of riverborne turbidity currents and indications of
888 slope failures in the Rhone delta of Lake Geneva. *Limnol. Oceanog.* **33**, 458-468 (1988).

889

890 **Acknowledgements**

891 PJT discloses support for the research of this work from the U.K. Natural Environment
892 Research Council (NERC) (grant numbers NE/S010068/1, NE/R001952/1 and
893 NE/K011480/1). KLM acknowledges funding from NIWA Marine Geological Resources
894 Programme and Marsden Grant 21-NIW-014). SH has received funding from the European
895 Union's Horizon 2020 research and innovation programme under the Marie Skłodowska-
896 Curie grant agreement No 899546. MAC acknowledges funding from the Natural
897 Environment Research Council (NERC) including National Capability Programme
898 (NE/R015953/1) "Climate Linked Atlantic Sector Science" (CLASS), "Environmental Risks
899 to Infrastructure: Identifying and Filling the Gaps" (NE/P005780/1) and "New field-scale
900 calibration of turbidity current impact modelling" (NE/P009190/1).

901

902 **Contributions**

903 PJT wrote the initial manuscript, with comments from all other authors. All authors played a
904 leading role in collection and analysis of direct flow monitoring data.

905

906 **Competing Interests**

907 The authors have no competing interests.

908

909 **Key Points**

- 910
- It was once thought that submarine turbidity currents were impractical to monitor in action, but detailed monitoring is now possible, and it is revealing major new insights.
- 911
- 912
- Monitoring identifies new triggers for flows, such as from very dilute river plumes, and consistently shows turbidity currents are much more frequent than predicted by
- 913
- past (e.g. sequence stratigraphic) models.
- 914
- Due to turbidity currents, the global burial efficiency of terrestrial organic carbon (28-45%) in marine sediments is significantly higher than previous estimates, and even
- 915
- higher (> 60-80%) during glacial low-stands.
- 916
- Faster (> ~1.5 m/s) turbidity currents are driven by a dense (10-30% concentration) near-bed layer at their front, which needs inclusion in flow modelling, whilst slower
- 917
- flows are entirely dilute.
- 918
- This dense frontal layer sometimes erodes large sediment volumes (as for ignition), yet maintains a near-uniform speed (as for autosuspension), leading to a new
- 919
- (travelling wave) model for flow behaviour.
- 920
- Monitoring shows how flows sculpt canyons and channels via supercritical bedforms (cyclic steps) and extremely fast-moving knickpoints that are internally generated, and
- 921
- how deposits record flow processes (e.g. cyclic steps).
- 922
- 923
- 924
- 925
- 926
- 927
- 928

929 **Glossary**

930

931 *Turbidity current*: An underwater avalanche of sediment and water that is denser than the
932 surrounding water, and thus moves down-slope along the ocean or lake floor.

933

934 *Turbidite*: Layer of sand and mud that has settled out from a turbidity current to form a
935 deposit on the ocean or lake floor.

936

937 *Ignition*: Positive feedback leading to acceleration of a turbidity current due to seafloor
938 erosion that causes the flow to become even faster and denser, leading to more erosion.

939

940 *Autosuspension*: A near-equilibrium state that occurs when settling of sand and mud from a
941 turbidity current is balanced by seafloor erosion, leading to near uniform flow velocity.

942

943 *Dissipation*: Negative feedback loop leading to deceleration of a turbidity current, as settling
944 of sand and mud causes the flow to become less-dense and slower, causing further settling.

945

946 *Acoustic Doppler current profiler (ADCP)*: Sensor emitting a sound-pulse that is scattered
947 from sand and mud particles within a turbidity current, which measures the speed of those
948 particles at different heights above the seabed to produce a velocity profile.

949

950 *Frontal cell*: The frontal part of faster-moving ($> \sim 1.5$ m/s) turbidity current that is faster
951 than the rest of the flow, and contains a near-bed layer with high sediment concentrations.

952

953 *Knickpoint*: An abrupt step in a submarine channel or canyon profile that resembles a water-
954 fall.

955

956 *Supercritical flow*: Flows can exist in two basic states that are either thin-and-fast
957 ('supercritical') flow or thick-and-slow ('subcritical') flow, which are separated by a
958 hydraulic jump.

959

960 *Submarine fan*: A large-scale accumulation of sediment formed by turbidity currents that
961 comprises a canyon, channel with levees, and lobe at the end of the channel.

962

963 *Submarine canyon:* A valley that is deeply incised into the seafloor through which turbidity
964 currents flow, which is much deeper than a submarine channel.

965

966 *Submarine channel:* A channel that is less deeply incised into the seafloor through which
967 turbidity currents flow, whose upraised flanks (called levees) may lie above the surrounding
968 seabed.

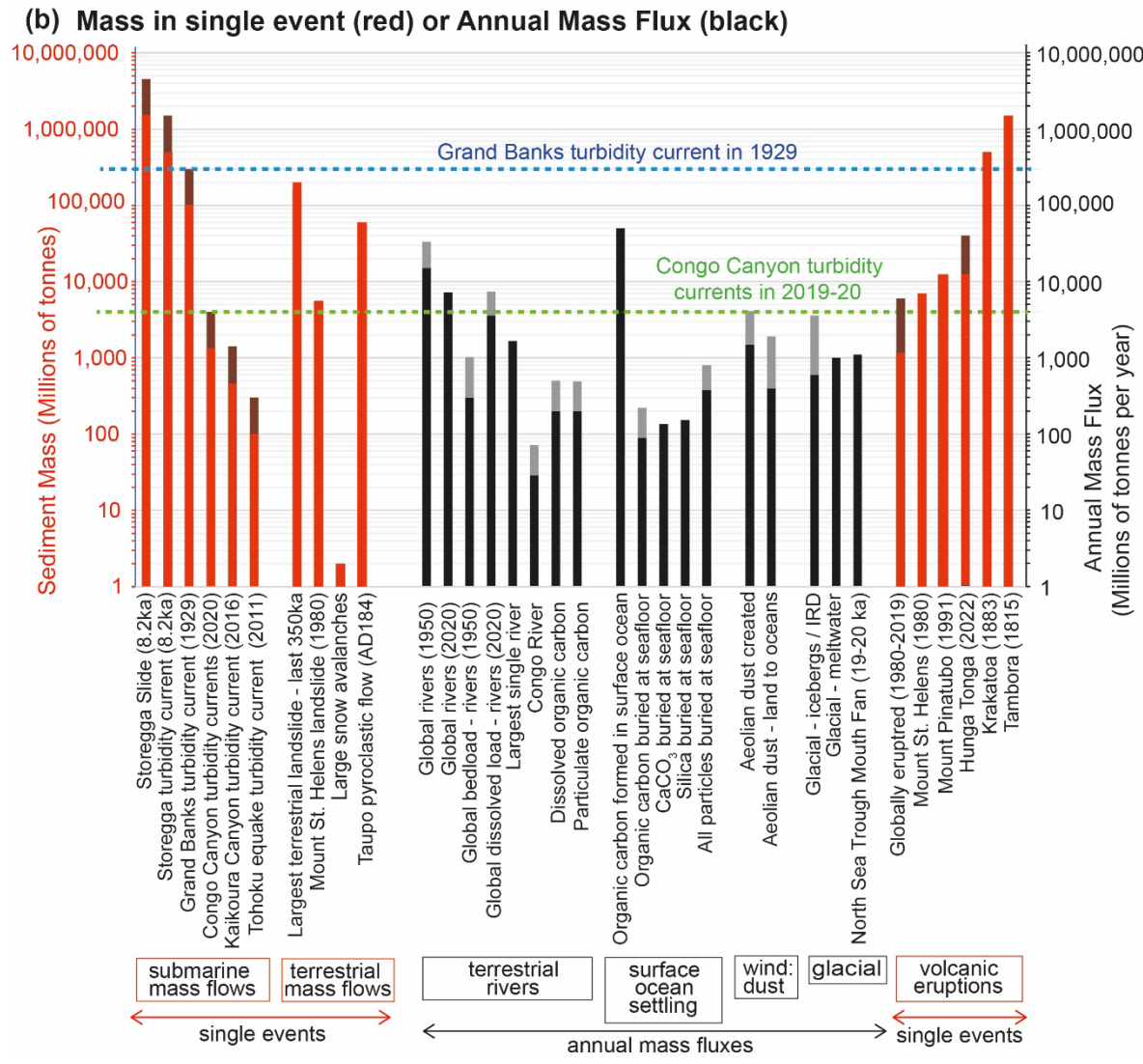
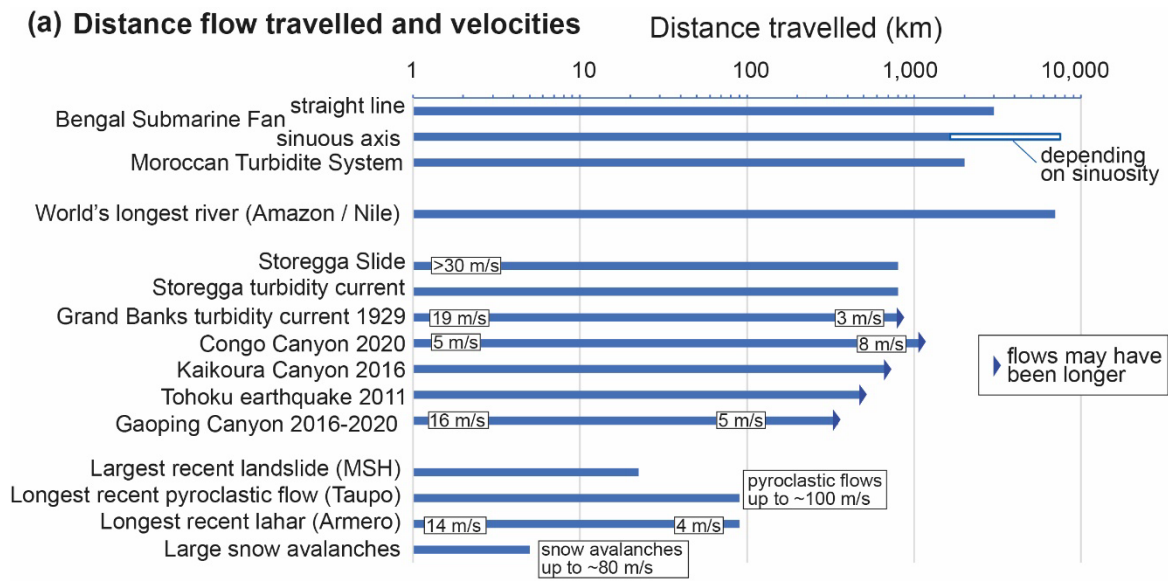
969

970 *Levee:* Upraised flanks of a submarine channel that lie above the surrounding seafloor, which
971 are formed by overspill of turbidity currents from the channel.

972

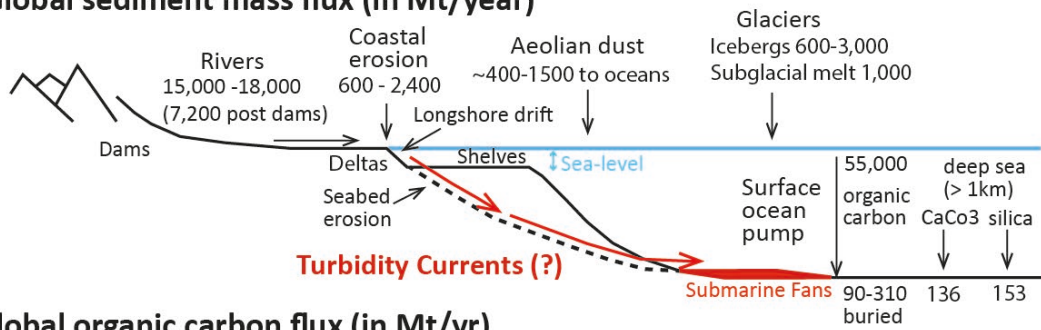
973 *Lobe:* Area that lies beyond the end of a submarine channel, where turbidity currents expand,
974 and which is often characterised by unusually rapid sediment deposition and scours.

975

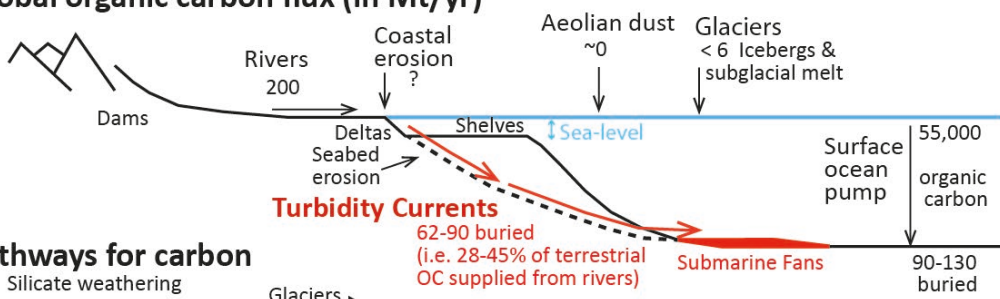


979 **Figure 1. Comparison between turbidity currents and various other major global**
980 **sediment transfer processes, showing turbidity current are one of the most important**
981 **sediment transfer processes ('pumps') on Earth. (a)** Distance that flows travel (km) and
982 their velocities (m/s). **(b)** Mass of sediment carried by individual events (in red), and as
983 annual sediment mass fluxes (in black), with uncertainties as grey additional bars. The
984 sediment mass carried by the Grand Banks turbidity current in 1929 (blue dotted line; [3])
985 and Congo Canyon turbidity currents in 2020 (green dotted line; [4]) are indicated.
986 Supplementary Table 1 provide further information and lists source literature used for the
987 distances, speeds, masses or annual mass fluxes that are quoted.
988
989

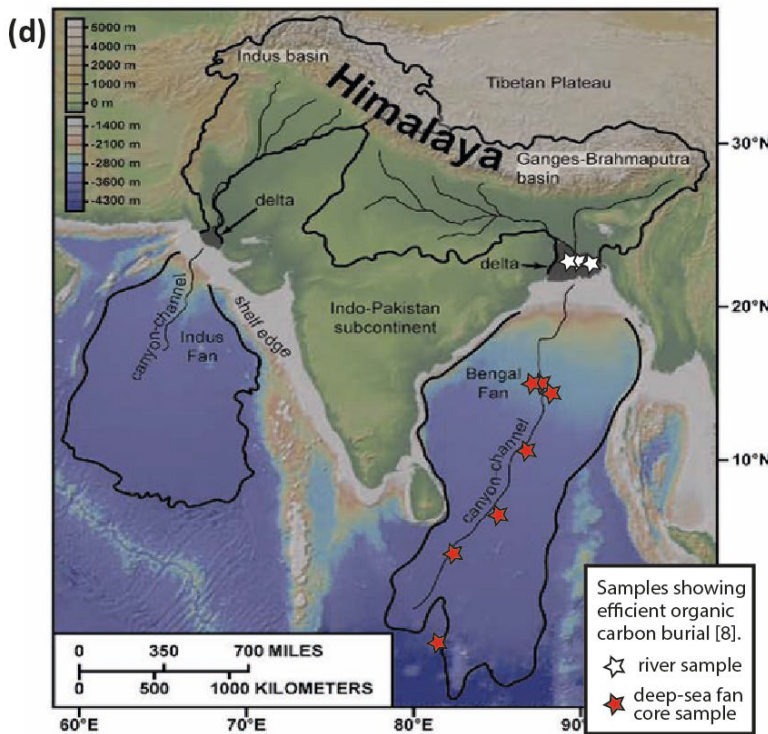
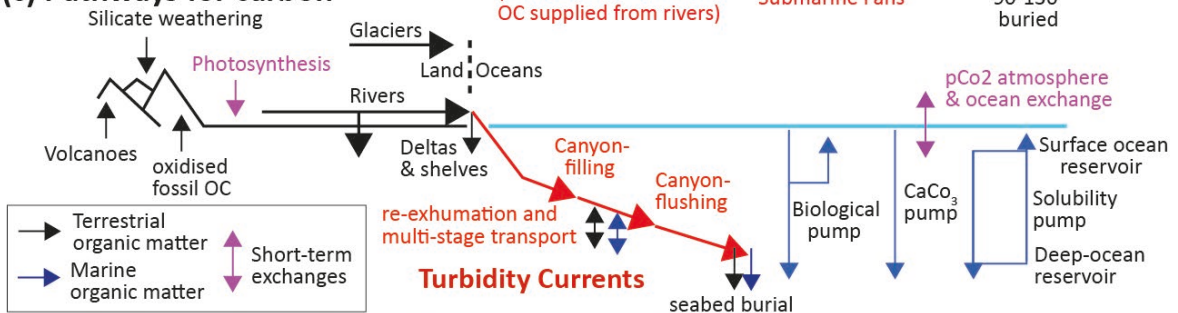
(a) Global sediment mass flux (in Mt/year)



(b) Global organic carbon flux (in Mt/yr)



(c) Pathways for carbon

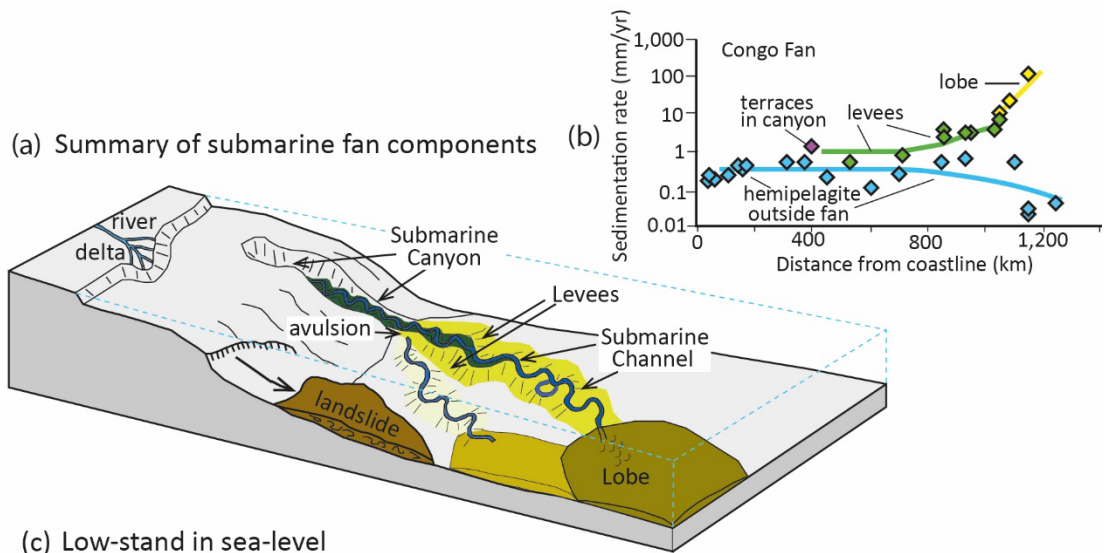


990

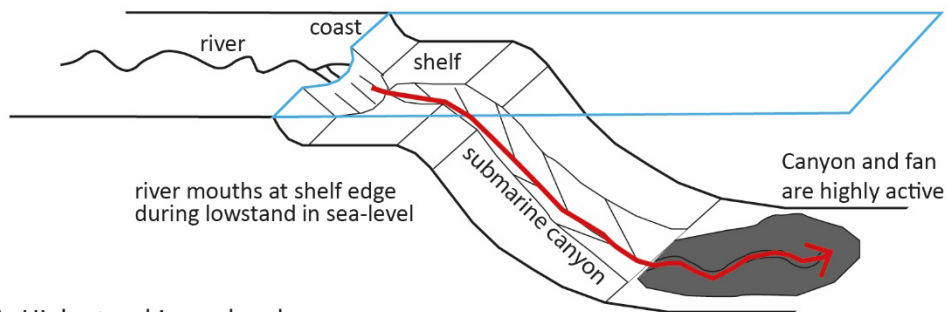
991 **Figure 2. Turbidity current play a globally important role in organic carbon burial. (a)**

992 Global sediment mass fluxes (in Mt/yr; see Figure 1 and Supplementary Table 1 for original

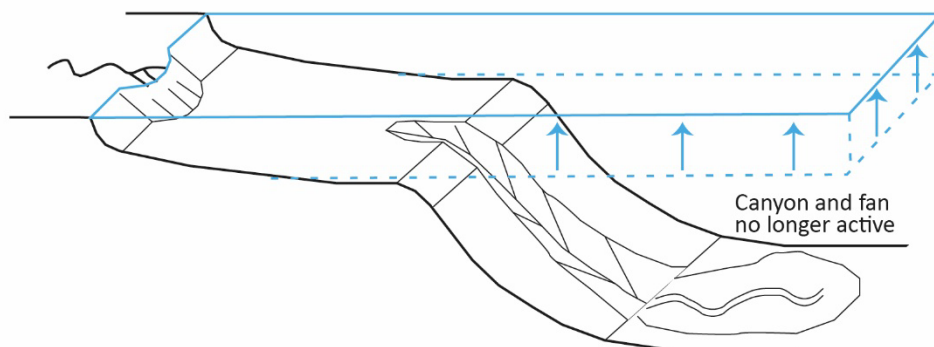
993 data sources). **(b)** Global organic carbon mass fluxes (in Mt/yr). A future grand challenge is
994 to quantify global sediment and organic carbon fluxes in turbidity currents [14]. **(c)** Pathways
995 for global organic carbon cycling. Burial of organic carbon by turbidity currents affects
996 atmosphere pCO₂ and thus climate, but over long term (> 1 ka) time scales. Terrestrial
997 organic carbon pathways in black, and marine organic carbon pathways in blue. Processes
998 that exchange carbon with atmosphere on short term in purple. Estimate of terrestrial organic
999 carbon burial (62-90 MtC/yr) in marine sediments by turbidity currents is from [14]. **(d)**
1000 Burial of organic carbon by turbidity currents can be highly efficient, such as within the huge
1001 Bengal Submarine Fan [8]. Organic carbon types and amounts in river samples (white stars)
1002 resemble those in deep-sea cores (red stars). Bathymetry data reproduced from the
1003 GEBCO_2021 Grid, www.gebco.net



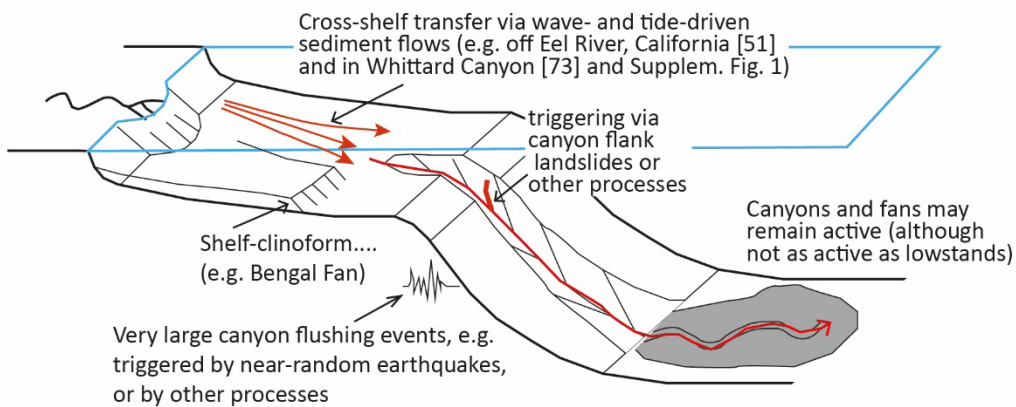
(c) Low-stand in sea-level



(d) High-stand in sealevel

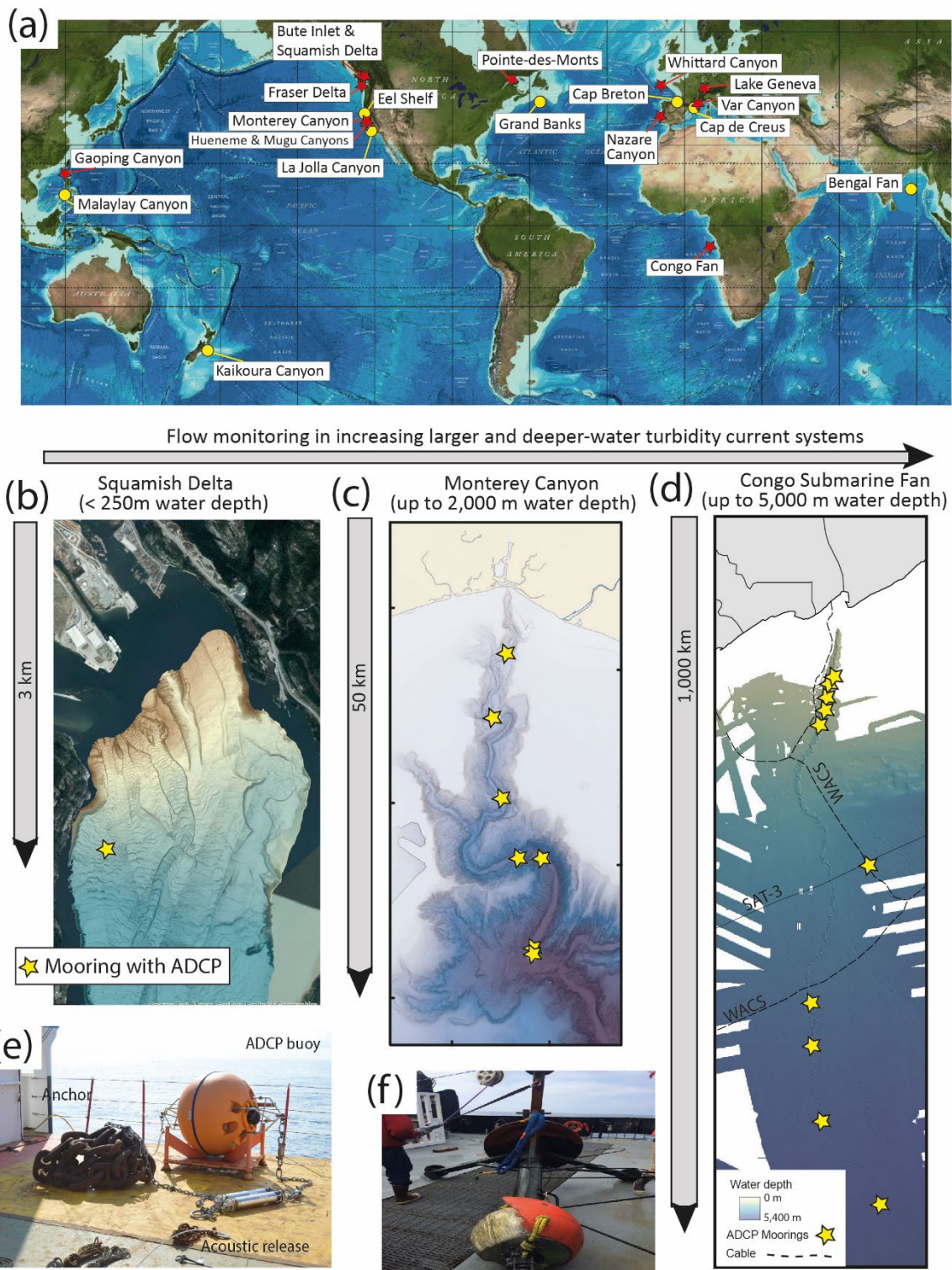


(e) Emerging understanding that turbidity current systems may not be dormant during current highstand in sealevel, as sediment may reach some canyon heads



1005 **Figure 3. Submarine fans and frequency of turbidity current activity.** (a) Summary of
1006 the main elements of a submarine fan. (b) Sedimentation rates in different parts of the Congo
1007 Submarine Fan (after [124]). (c) At glacial low-stands in sea-level, most river mouths will
1008 connect directly to submarine canyon-heads [67,68], so that turbidity currents are highly
1009 active on submarine fans [66,70]. This is also the case for the small number of modern
1010 canyon-heads that connect directly to river mouths (e.g. Congo Canyon [4] or Gaoping
1011 Canyon [9,41,42]). (d) Previous sequence (e.g. stratigraphic models) proposed that submarine
1012 canyons are dormant during high-stands in sea-level [66], as river mouths are separated from
1013 most canyon heads. (e) However, there is an emerging view that turbidity current systems are
1014 surprisingly active during the present day high-stand in sea-level [70]. For example, turbidity
1015 currents occur in Whittard Canyon, despite being 300 km from the nearest coast [69], and
1016 flows occur for 30% of the time in the upper Congo Canyon [36, 37] (Supplementary Fig. 2).
1017 Sediment can also be transferred efficiently across the shelf via wave or tide action to the
1018 canyon head (e.g. Eel Shelf in California) [73,74], or via progradation of large clinofolds
1019 (e.g. Bengal Fan in the Bay of Bengal) [72].

1020



1021

1022 **Figure 4. Direct monitoring of turbidity currents.** (a) Map of just ~12 locations (red stars)

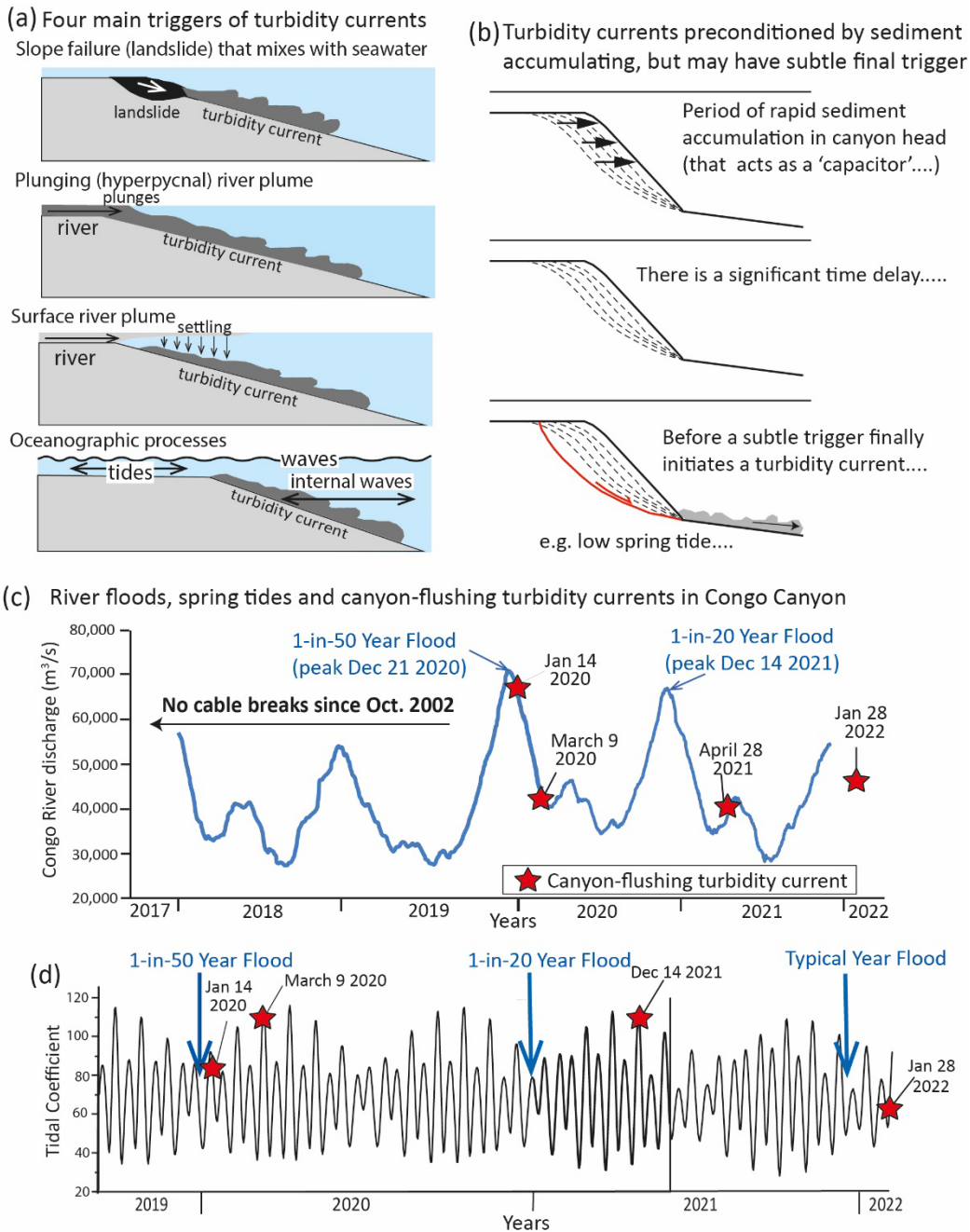
1023 worldwide where turbidity currents have currently been monitored in detail [27-54,61,69,

1024 125-126] and other key locations (yellow circles) mentioned in the text. Image reproduced

1025 from the GEBCO world map 2014, www.gebco.net. Flow monitoring has moved from (b)

1026 smaller systems in shallow water such as Squamish Delta [38-39,50,59,61,115] where

1027 logistic are easier, to **(c)** larger systems in moderate depths such as Monterey Canyon
1028 [34,35,51-52,60,87], and **(d)** finally very large systems in deep-water such as the Congo Fan,
1029 where turbidity currents broke the WACs and SAT-3 telecommunication cables (dotted lines)
1030 in 2020 and 2021 [4,36,37]. **(e)** These studies included moorings with an acoustic Doppler
1031 current meter (ADCP) in a buoyant float connected to a heavy (e.g. 1 tonne) anchor via a
1032 wire or chain, and recovered by remote triggering of an acoustic release [118]. Mooring
1033 shown here is on deck of a research vessel before deployment in Congo Canyon. **(f)** Heavy
1034 frame weighing 800 kg that slid for ~7 km down Monterey Canyon at speeds of up to 4.4 m/s
1035 [35,52]. It moved at a similar speed to much smaller objects, suggesting that they were rafted
1036 in a dense near-bed layer [35,52].
1037



1039

1040

1041

1042

1043

1044

1045

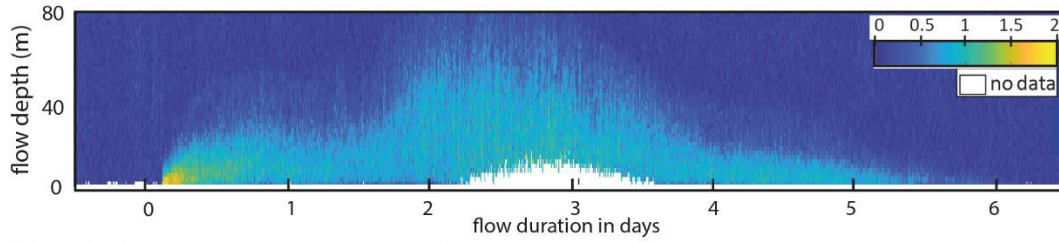
1046

1047

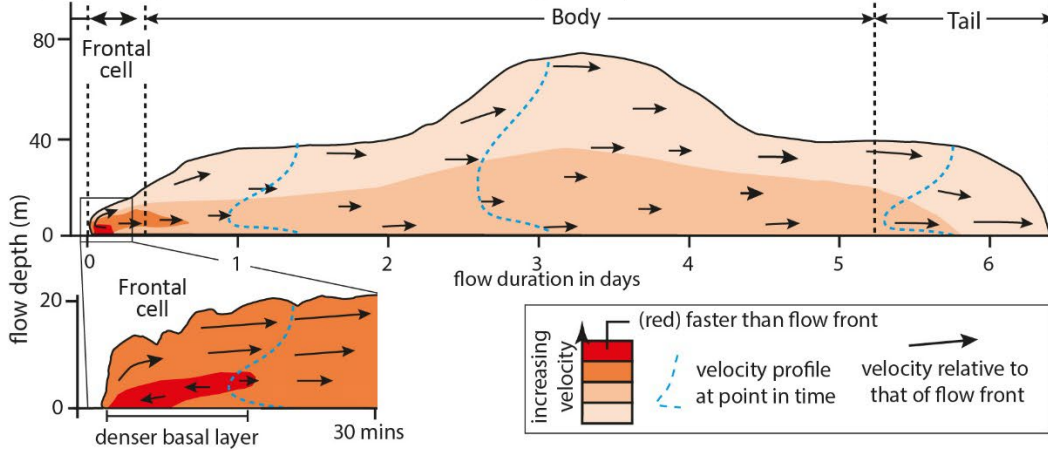
Figure 5. New insights into causes of turbidity currents. (a) Four main causes of turbidity currents [55,56] are (i) slope failures (landslides), (ii) plunging of hyperpycnal river plumes that have high enough sediment concentrations to be denser than seawater [57], and (iii) sediment settling from surface river plumes [39,47-48,58]. It has emerged that surface river plumes with very low (< 0.07 g/l) sediment concentrations can generate turbidity currents [39], such that turbidity currents may occur offshore a wider range of rivers than once thought. (iv) Oceanographic processes such as storm waves, tides and internal waves that can

1048 supply sediment to canyon heads and trigger flows (including via landslides). **(b)** Significant
1049 time delays may occur between periods of rapid sediment accumulation in canyon heads, and
1050 final triggering of turbidity currents by subtle external triggers [4,60-61]. **(c,d)** River floods
1051 and tides combine to generate turbidity currents at many sites worldwide, including four
1052 extremely powerful turbidity currents (red stars) that flushed the Congo Canyon in 2020-2022
1053 [4,5]. This cluster of canyon-flushing turbidity currents are associated with major floods
1054 along the Congo River, but occurred several weeks to months after the flood peaks, often at
1055 spring tides [4,5].

a) Turbidity current velocity data measured in the Congo Canyon

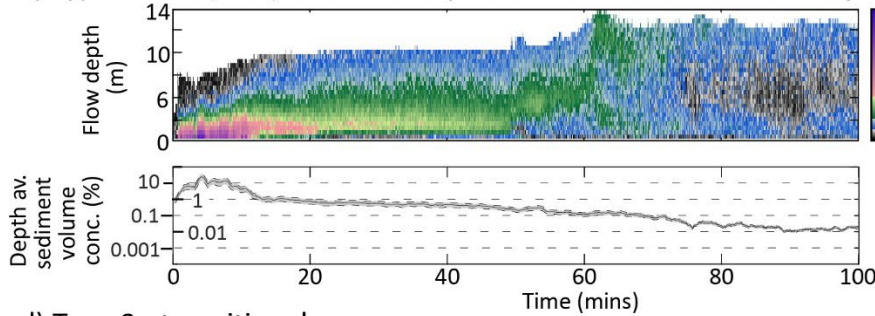


b) Turbidity current structure in the Congo Canyon

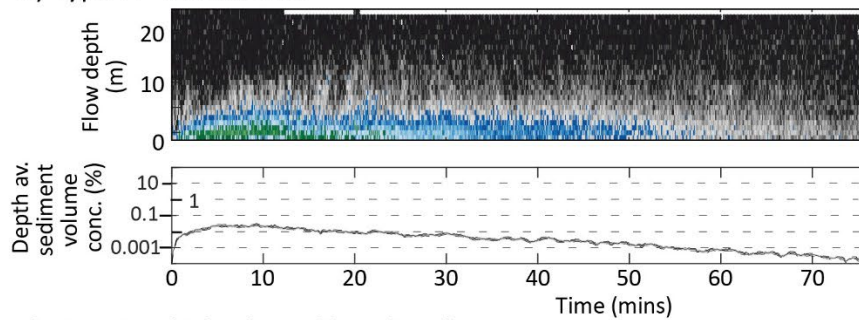


Three types of turbidity current structure in Bute Inlet

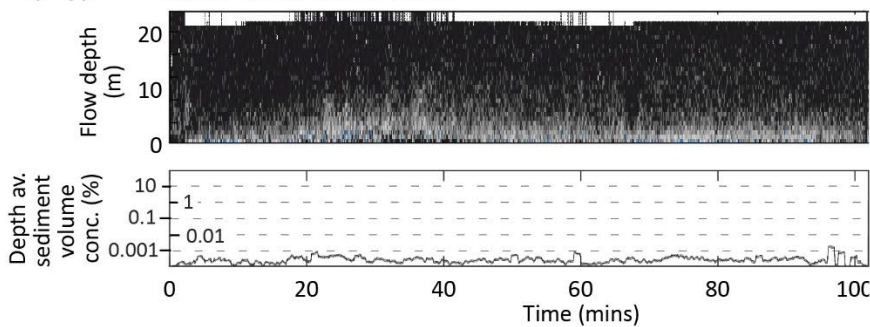
c) Type 1 - thin, fast, dense head (frontal cell with dense basal layer)



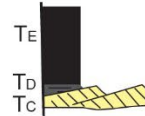
d) Type 2 - transitional



e) Type 3 - thick, slow, dilute head



Inferred deposit types

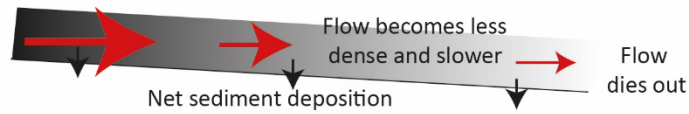


1057

1058 **Figure 6. New insights into internal structure of turbidity currents.** (a) Velocity time-
1059 series of a turbidity current in Congo Canyon measured by an ADCP mooring [after 36]. (b)
1060 Summary of velocity structure of Congo Canyon turbidity currents. They comprise a near-
1061 bed frontal zone ('frontal cell') that is faster and denser than the rest of the flow, and runs
1062 away from a trailing body and tail, causing the flow to stretch [36]. This structure differs
1063 from laboratory flows in which a faster body feeds a slower head [33]. (d-f) Three types of
1064 turbidity currents observed in Bute Inlet. Plots show time-series of velocity and layer-average
1065 sediment volume concentration derived via the Chezy equation [after 40]. Faster (>1.7 m/s)
1066 Type 1 flows have a frontal cell with a fast and dense near-bed layer, as in Congo Canyon
1067 flows. This dense layer drives the event and dominates sediment flux [40]. Slower Type 3
1068 flows are entirely dilute, and lack a dense and fast frontal layer, whilst type 2 flows have
1069 intermediate speeds and sediment concentrations. A single turbidity current may evolve from
1070 Type 1 to Types 2 and 3 as it decelerates [40]. (f) Inferred types of turbidite deposit likely
1071 formed by different types of flow, with Bouma sequence intervals (T_A to T_E) marked [40].

1072

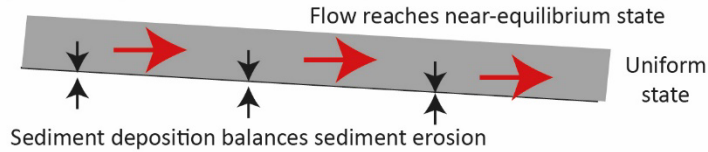
(a) **Dissipation: flow deposits, becomes less dense and decelerates**



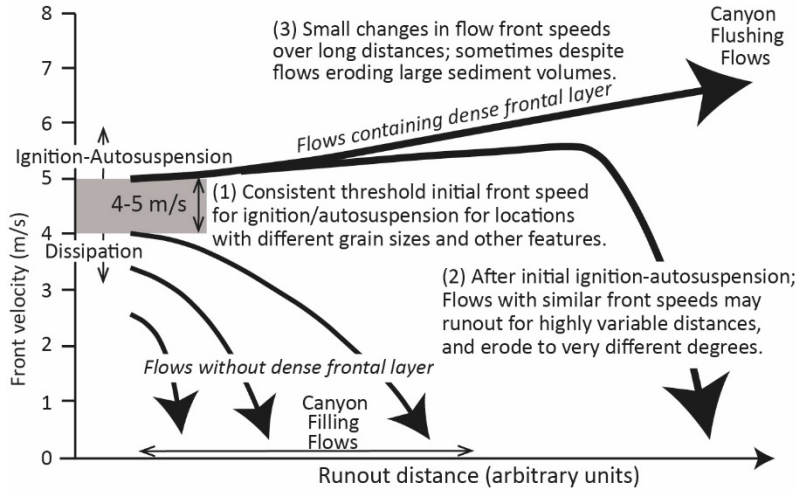
(b) **Ignition: flow erodes, becomes denser and accelerates**



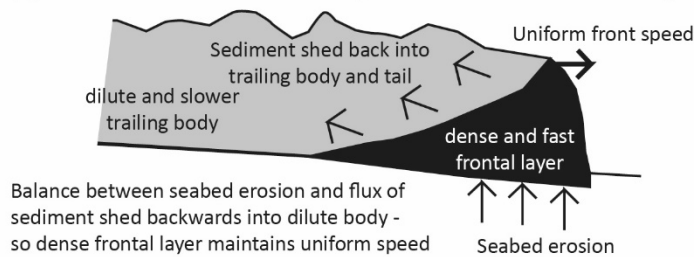
(c) **Autosuspension: erosion & deposition balance, uniform speed**



(d) **Velocity-distance diagram summarizing turbidity current behaviour**



(e) **New model: flow is erosive yet has near-uniform front speed**



1074

1075

1076 **Figure 7. A new view of how turbidity currents behave.** Past models inferred flows either
 1077 **(a)** deposited sediment and dissipated; **(b)** eroded, became denser and faster, and accelerated
 1078 (ignited); or **(c)** balanced erosion and deposition to create a near-equilibrium uniform velocity
 1079 (autosuspending) state [25]. Red arrows denote flow speed; black arrows are sediment
 1080 exchange with the bed. **(d)** Summary of changes in flow front speeds seen in direct field
 1081 measurements, showing how flow behaviour diverges if an initial threshold speed of 4-5 m/s

1082 is exceeded [4,87]. The threshold speed is independent of dominant sediment grain size. (e)
1083 New 'travelling wave' model in which flows may both erode the seabed (as in ignition) and
1084 sustain near uniform speeds for long distances (as in autosuspension) [4,87]. The flow
1085 contains a dense frontal layer in which seabed erosion is balanced by sediment shed back into
1086 a dilute trailing body.